PHYSICAL REVIEW B VOLUME 43, NUMBER 2 15 JANUARY 1991-I

Detailed surface and gas-phase chemical kinetics of diamond deposition

Michael Frenklach and Hai Wang
Department of Materials Science and Engineering, Pennsylvania State University, University Park, Pennsylvania 16802
(Received 29 March 1990; revised manuscript received 10 September 1990)

A chemical kinetic model is developed that includes detailed descriptions of both gas-phase and surface processes occurring in gas-activated deposition of diamond films on diamond (111) surface. The model was tested by simulating diamond film deposition in a hot-filament reactor using methane-hydrogen, methane-argon, and methane-oxygen-hydrogen gas mixtures. The gas-phase part of the model includes transport phenomena and predicts correctly the measured concentrations of major gaseous species. The surface part of the model reproduces the general experimental trends—the effects of temperature, pressure, initial methane concentration, and the addition of oxygen—for the growth rate and film quality. Analysis of the computational results revealed the factors controlling the growth phenomena. Among several reaction pathways describing deposition of diamond initiated by different gaseous species, including CH_3 and several C_2H_x species, the H-abstraction–C_2H_2-addition mechanism appears to dominate. The key role of hydrogen and oxygen is identified to be the suppression of the formation of aromatic species in the gas phase, which prevents their condensation on the deposition surface. Activation of the growing surface by H atoms and gasification of sp^2 carbon by OH radicals are other important factors. The developed model does not support the theory of preferential etching by H atoms advanced to explain the kinetic competition between diamond and nondiamond phases. Instead, it establishes the critical role of aromatics condensation and interconversion of sp^2 and sp^3 carbon phases mediated by hydrogen atoms.

I. INTRODUCTION

The technique of chemical vapor deposition (CVD) of diamond films at low pressures has advanced rapidly in recent years.[1–5] The deposition rates and film quality are repeatedly demonstrated to be sufficiently high for a number of commercial applications to be feasible.[6] At the same time, it becomes evident that further technological advancement, particularly in such challenging areas as single-crystal growth for electronic applications[7] and low-temperature deposition for coating of optic and plastic materials,[8] requires a detailed understanding of the fundamental phenomena responsible for diamond nucleation and growth.

The Russian school of Derjagin, Fedoseev, and coworkers[9–12] developed a model for diamond nucleation and growth based on macroscopic concepts of classical nucleation theory and adsorption-desorption kinetics and equilibrium. Their theory, however, does not identify possible growth species or specific reactions taking place at the surface; it is formulated in rather vague terms of surface coverage, the formation of surface complexes, and the etching of graphite by atomic hydrogen. Similar thermodynamic and classical nucleation approaches have been suggested by others.[5,13–16] Several research groups have begun using detailed chemical kinetic modeling to describe gas-phase reactions occurring in diamond deposition processes;[17–23] however, surface processes were treated in a very general, phenomenological manner. Tsuda *et al.*[24,25] and Huang *et al.*[26] investigated the energetics of several elementary surface reactions, but no kinetic modeling was attempted.

Here we report a detailed kinetic modeling of surface processes occurring in diamond CVD. The deposition is described in terms of elementary chemical reactions for both gas-phase and surface phenomena. Diffusion of chemical species and gas convection are also included. The model is tested by simulating diamond film deposition in a hot-filament reactor using methane-hydrogen, methane-argon, and methane-oxygen-hydrogen gas mixtures. The computational results are then analyzed, revealing the factors controlling the growth phenomena.

II. COMPUTATIONAL DETAILS

A. Model

The assumed model is an idealized constant-diameter hot-filament reactor and, computationally, consists of two separate submodels, those simulating the gas-phase and the surface reactions. The gas-phase submodel is a constant pressure laminar flow with an imposed temperature profile. The reactor conditions—initial mixture composition, pressure, initial gas velocity, and temperature profile—were founded on the experimental data of Harris *et al.*[27] For the "base" case in this work, we chose a (0.3 vol. % CH_4)-H_2 mixture, pressure 20 Torr, linear gas velocity 0.5 cm/s (at the temperature of 2600 K), and the temperature profile shown in Fig. 1. The latter was obtained by numerically fitting the measurements[27] downstream the filament and assuming, for the lack of experimental data, that the temperature profile upstream the filament is symmetrical to the downstream profile and that the gas remains in contact with the fila-

ment for a finite period of time at a constant temperature of 2600 K. The inclusion of the upstream portion of the temperature profile was found to be necessary for correct prediction of downstream species concentrations. As no other experimental data are available, the temperature profile obtained in this manner was used in all the simulations reported here. This is justifiable because the hydrocarbon mixtures considered in the present study have an extremely large, greater than 96%, degree of dilution and therefore the temperature differences among such mixtures should be small.

The reactive gas composition was computed using the Sandia burner code,[28] which solves the conservation equations for mass, momentum, and species concentrations in a one-dimensional gas flow with an assumed temperature profile, accounting for chemical reactions, species diffusion (including thermal diffusion), and gas convection. The ideal gas law was assumed throughout. The transport properties were computed using the code and data of Kee *et al.*[29] For chemical species not specified in the latter data base, the required Lennard-Jones parameters were calculated using empirical correlations and available physical properties.[30] The reaction mechanism, rate coefficients, and thermodynamic data assumed are presented in Sec. II B below.

In the surface submodel, we assumed that the film is deposited on a substrate placed along the reactor wall and that the deposition surface is in local thermal equilibrium with the gas. The deposition process is described by a set of elementary chemical reactions of surface sites. The rates of these reactions are expressed in terms of two-dimensional concentrations of surface sites and diffusional fluxes of gaseous species produced in the gas-phase reactions. It was assumed that the gas-phase concentrations of chemical species are unaffected by their consumption or production in the surface reactions, and the computational results fully supported this assumption. The evolution of the surface sites was obtained by numerical integration of a set of simultaneous ordinary differential equations describing the kinetics of the developed reaction mechanism. A complete list of the surface reactions, corresponding rate coefficients, and details on the estimation techniques are given in Sec. II C below. The numerical integration of the differential equations was performed with an in-house computer code using the LSODE integrator of Hindmarsh.[31]

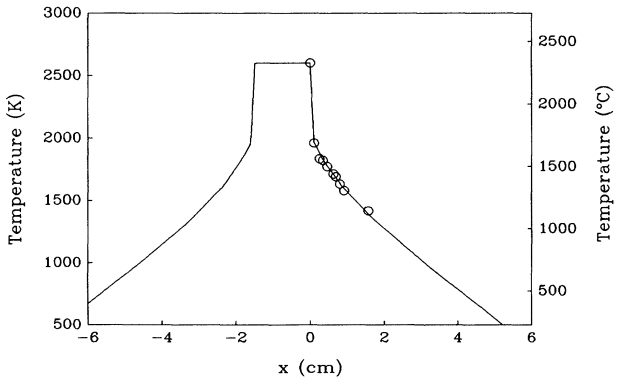

FIG. 1. The assumed reactor temperature profile as a function of the distance from the filament. $x=0$ identifies the location of the filament. Circles indicate the measurements of Harris *et al.* (Ref. 27).

The overall computational procedure was organized in two steps. First, for a given set of initial conditions, the concentration profiles of the gas-phase species were computed with the burner code. The obtained species concentrations were then used as an input to the surface kinetic code. All computations were performed on an IBM 3090-600S computer at the Pennsylvania State University Center for Academic Computing.

B. Gas-phase reaction mechanism

The chemical reaction mechanism used in this work to describe the gas-phase kinetics is based on two mechanisms developed in our laboratory for applications in combustion and flamelike environments. The first is a 125-reaction, 31-species mechanism developed for high-temperature pyrolysis and oxidation of methane and optimized to reproduce quantitatively a variety of ignition and flame experiments.[32] The second is a 342-reaction, 70-species mechanism, which quantitatively describes the formation and growth of polycyclic aromatic hydrocarbons (PAH's) in acetylene and ethylene flames.[33] These two mechanisms were combined and reduced in size,[34] removing those reactions that do not contribute significantly at the conditions employed in the present study. The obtained 158-reaction, 50-species mechanism, along with the assigned temperature- and pressure-dependent rate coefficients, is given in Table I.

Reactions $(g9)$–$(g68)$ in Table I describe the conversion of methane into methyl radical, ethane, ethylene, acetylene, and other C_1H_x and C_2H_y gaseous species; reactions $(g69)$–$(g129)$ describe the formation of larger aliphatics; and reactions $(g130)$–$(g158)$ the formation of aromatics. To assist the reader in the identification of large hydrocarbons, coded in Table I following our compact nomenclature,[88] the structures of several key chemical species are specified explicitly in Table II. The nomenclature for the rest of the C_4H_x and larger hydrocarbon compounds can be found in Frenklach *et al.*[88,89] species $^{(3)}CH_2$ and $^{(1)}CH_2$ denote the triplet electronic ground ($\tilde{X}\,^3B_1$) and low-lying singlet first excited ($\tilde{a}\,^1A_1$) states of the methylene radical, respectively.

For pressure-dependent reactions, three rate coefficient expressions—for the three pressures used in this study—are given in Table I. Most of these expressions are calculated using the Troe-Golden formalism[84–86] in the form reported by us previously.[18] The collision efficiency for the bath gas H_2 was taken from the literature whenever available or otherwise assumed to be equal to 2.9, relative to the collision efficiency of argon, or 2.5, relative to the collision efficiency of N_2.[35] The principle of detailed balancing was obeyed for all reactions except for those whose detailed mechanism remains unknown: oxidation of aromatic molecules by OH and oxidation of ethynyl, vinyl, and aromatic radicals by O_2. The thermo-

TABLE I. Gas-phase reaction mechanism.

No.	Reaction[a]		Forward rate coefficient[b] A	n	E	References and/or comments
	H_2/O_2 reactions					
$g1$	$H+H+M \rightleftarrows H_2+M$		9.70[+16]	−0.60		35, $M=H_2$
$g2$	$H+O_2 \rightleftarrows OH+O$		1.59[+17]	−0.927	70.6	36
$g3$	$O+H_2 \rightleftarrows OH+H$		3.87[+04]	2.70	26.2	37
$g4$	$OH+H_2 \rightleftarrows H_2O+H$		2.16[+08]	1.51	14.4	38
$g5$	$H+OH+M \rightleftarrows H_2O+M$		2.20[+22]	−2.00		35, $M=H_2$
$g6$	$H+O_2+M \rightleftarrows HO_2+M$		2.80[+18]	−0.80		39, $M=H_2$
$g7$	$HO_2+H \rightleftarrows OH+OH$		1.50[+14]		4.2	35
$g8$	$HO_2+H \rightleftarrows H_2+O_2$		2.50[+13]		2.9	35
	Decomposition of CH_4					
$g9$	$CH_4 \rightleftarrows CH_3+H$	10 Torr	3.08[+32]	−6.09	450.4	c
		20 Torr	1.34[+33]	−6.18	452.0	c
		50 Torr	1.31[+34]	−6.34	455.2	c
$g10$	$CH_3+H_2 \rightleftarrows CH_4+H$		4.13[+04]	2.50	39.4	32
$g11$	$CH_4+OH \rightleftarrows CH_3+H_2O$		1.50[+06]	2.13	10.2	42
$g12$	$CH_4+O \rightleftarrows CH_3+OH$		1.90[+09]	1.44	36.3	43
	Reactions of CH_3					
$g13$	$CH_3+H \rightleftarrows {}^{(3)}CH_2+H_2$		1.80[+14]		63.2	44
$g14$	$CH_3+OH \rightleftarrows {}^{(3)}CH_2+H_2O$		1.13[+06]	2.13	10.2	32
$g15$	$CH_3+OH \rightleftarrows CH_2O+H_2$		8.00[+12]			44
$g16$	$CH_3+O \rightleftarrows CH_2O+H$		8.43[+13]			45
$g17$	$CH_3+O_2 \rightleftarrows CH_2O+OH$		7.58[+11]		37.4	32
$g18$	$CH_3+M \rightleftarrows {}^{(3)}CH_2+H+M$		2.90[+16]		379.0	35, $M=H_2$
	Reactions of CH_2O					
$g19$	$CH_2O+H \rightleftarrows CHO+H_2$		1.26[+08]	1.62	9.1	46
$g20$	$CH_2O+OH \rightleftarrows CHO+H_2O$		7.23[+05]	2.46	−4.1	47
$g21$	$CH_2O+CH_3 \rightleftarrows CHO+CH_4$		8.91[−13]	7.40	−4.0	48
$g22$	$CH_2O+M \rightleftarrows CHO+H+M$		1.45[+17]		320.0	35, $M=H_2$
$g23$	$CH_2O+M \rightleftarrows CO+H_2+M$		2.40[+16]		291.0	44, $M=H_2$
	Reactions of CHO					
$g24$	$CHO+H \rightleftarrows CO+H_2$		2.00[+14]			35
$g25$	$CHO+OH \rightleftarrows CO+H_2O$		1.00[+14]			39
$g26$	$CHO+M \rightleftarrows CH+H+M$		3.48[+17]	−1.00	71.1	49, $M=H_2$
	CO/CO_2 reactions					
$g27$	$CO+OH \rightleftarrows CO_2+H$		1.05[+07]	1.37	−3.0	d
$g28$	$CO+O+M \rightleftarrows CO_2+M$		7.10[+13]		−19.0	35
	Formation and consumption of C_2H_6					
$g29$	$C_2H_6 \rightleftarrows CH_3+CH_3$	10 Torr	2.37[+42]	−8.88	451.7	e
		20 Torr	5.52[+42]	−8.90	452.1	e
		50 Torr	2.20[+43]	−8.95	453.2	e
$g30$	$C_2H_6+H \rightleftarrows C_2H_5+H_2$		5.40[+02]	3.50	21.8	35
$g31$	$C_2H_6+OH \rightleftarrows C_2H_5+H_2O$		2.20[+07]	1.90	4.7	52
$g32$	$C_2H_6+CH_3 \rightleftarrows C_2H_5+CH_4$		5.50[−01]	4.00	34.7	35
	Reactions of C_2H_5					
$g33$	$CH_3+CH_3 \rightleftarrows C_2H_5+H$	10 Torr	4.39[+12]	0.11	44.6	e
		20 Torr	4.64[+12]	0.11	44.7	e
		50 Torr	5.62[+12]	0.08	45.2	e
$g34$	$C_2H_5+H \rightleftarrows C_2H_4+H_2$		3.00[+13]			35
$g35$	$C_2H_5 \rightleftarrows C_2H_4+H$	10 Torr	1.30[+37]	−8.15	184.3	f
		20 Torr	6.28[+37]	−8.24	186.9	f
		50 Torr	1.25[+38]	−8.20	189.4	f

TABLE I. (*Continued*).

No.	Reaction[a]		Forward rate coefficient[b] A	n	E	References and/or comments
	Formation and consumption of C_2H_4					
g36	$CH_3+{}^{(3)}CH_2 \rightleftarrows C_2H_4+H$		5.00[+13]			54
g37	$C_2H_4+H \rightleftarrows C_2H_3+H_2$		3.16[+11]	0.70	33.5	55
g38	$C_2H_4+OH \rightleftarrows C_2H_3+H_2O$		2.70[+13]		24.9	g
g39	$C_2H_4+CH_3 \rightleftarrows C_2H_3+CH_4$		4.20[+11]		46.5	35
g40	$C_2H_4+M \rightleftarrows C_2H_2+H_2+M$		7.54[+17]		332.0	35, $M=H_2$
g41	$C_2H_4+M \rightleftarrows C_2H_3+H+M$		7.54[+17]		404.0	35, $M=H_2$
	Reactions of C_2H_3					
g42	$C_2H_3+H \rightleftarrows C_2H_2+H_2$		3.00[+13]			58
g43	$C_2H_3+OH \rightleftarrows C_2H_2+H_2O$		4.00[+12]			59
g44	$C_2H_3+O_2 \rightleftarrows CH_2O+CHO$		4.00[+12]		−1.0	60
g45	$C_2H_2+H \rightleftarrows C_2H_3$	10 Torr	7.18[+34]	−7.52	30.9	h
		20 Torr	3.12[+35]	−7.61	32.9	h
		50 Torr	1.13[+36]	−7.65	35.5	h
	Reactions of C_2H_2					
g46	$C_2H+H_2 \rightleftarrows C_2H_2+H$		8.00[+12]		11.0	35,62
g47	$C_2H_2+O \rightleftarrows {}^{(3)}CH_2+CO$		7.81[+03]	2.80	2.1	i
g48	$C_2H_2+O \rightleftarrows CHCO+H$		1.39[+04]	2.80	2.1	i
g49	$C_2H_2+OH \rightleftarrows C_2H+H_2O$		2.71[+13]		43.9	65
g50	$C_2H_2+OH \rightleftarrows CH_2CO+H$		2.19[−04]	4.50	−4.2	66
	Reactions of CH_2CO					
g51	$CH_2CO+H \rightleftarrows CHCO+H_2$		3.00[+13]		36.0	67
g52	$CH_2CO+M \rightleftarrows {}^{(3)}CH_2+CO+M$		1.00[+16]		248.0	35, $M=H_2$
	Formation and consumption of ${}^{(1)}CH_2$					
g53	$CHCO+H \rightleftarrows {}^{(1)}CH_2+CO$		1.50[+14]			64
g54	${}^{(1)}CH_2+H \rightleftarrows CH+H_2$		3.00[+13]			68
g55	${}^{(1)}CH_2+H_2 \rightleftarrows CH_3+H$		7.23[+13]			68
g56	${}^{(1)}CH_2+OH \rightleftarrows CH_2O+H$		3.00[+13]			68
g57	${}^{(1)}CH_2+O_2 \rightleftarrows CO+OH+H$		2.19[+13]			68
g58	${}^{(1)}CH_2+O_2 \rightleftarrows CO_2+H_2$		9.40[+12]			68
g59	${}^{(1)}CH_2+CH_3 \rightleftarrows C_2H_4+H$		1.80[+13]			68
g60	${}^{(1)}CH_2+M \rightleftarrows {}^{(3)}CH_2+M$		1.50[+13]			j, $M=H_2$
	Reactions of ${}^{(3)}CH_2$					
g61	${}^{(3)}CH_2+H \rightleftarrows CH+H_2$		4.00[+13]			35
g62	${}^{(3)}CH_2+OH \rightleftarrows CH_2O+H$		2.50[+13]			59
g63	${}^{(3)}CH_2+OH \rightleftarrows CH+H_2O$		1.13[+07]	2.00	12.6	59
g64	${}^{(3)}CH_2+O_2 \rightleftarrows CO+OH+H$		1.60[+12]		4.2	59
	Formation and consumption of C atoms					
g65	$CH+H \rightleftarrows C+H_2$		1.50[+14]			59
g66	$C+O_2 \rightleftarrows CO+O$		2.00[+13]			59
g67	$C+OH \rightleftarrows CO+H$		5.00[+13]			59
g68	$C+CH_3 \rightleftarrows C_2H_2+H$		5.00[+13]			59
	Formation and consumption of C_3H_x species					
g69	$CH+C_2H_2 \rightleftarrows C_3H_2+H$		1.10[+13]			69
g70	$C_3H_2+OH \rightleftarrows C_2H_2+CHO$		6.80[+13]			69
g71	$C_3H_2+H \rightleftarrows C_3H_3$		6.00[+12]			69
g72	${}^{(3)}CH_2+C_2H_2 \rightleftarrows C_3H_3+H$		1.20[+13]		27.7	70
g73	${}^{(1)}CH_2+C_2H_2 \rightleftarrows C_3H_3+H$		3.00[+13]			59
g74	$C_3H_3+OH \rightleftarrows C_2H_2+CH_2O$		2.00[+13]			k
g75	$C_3H_4+H \rightleftarrows C_3H_3+H_2$		1.00[+12]		6.3	71
g76	$C_3H_4+H \rightleftarrows CH_3+C_2H_2$		2.00[+13]		10.1	69
g77	$C_3H_4+OH \rightleftarrows CHO+C_2H_4$		5.00[+12]		5.4	69

TABLE I. (*Continued*).

No.	Reaction[a]		Forward rate coefficient[b] A	n	E	References and/or comments
	Formation and reactions of C_4H_x species					
g78	$C_2H_4+C_2H_3\rightleftarrows C_4H_6+H$		6.21[+11]		14.0	72
g79	$C_3H_4+{}^{(1)}CH_2\rightleftarrows C_4H_6$		2.00[+13]			estimated
g80	$C_4H_6+H\rightleftarrows n\text{-}C_4H_5+H_2$		6.30[+10]	0.70	25.1	55
g81	$C_4H_6+OH\rightleftarrows n\text{-}C_4H_5+H_2O$		2.20[+13]		17.5	$k_{g81}=k_{g93}$
g82	$n\text{-}C_4H_5+H\rightleftarrows C_4H_4+H_2$		1.50[+13]			$k_{g82}=k_{g42}/2$
g83	$n\text{-}C_4H_5+O_2\rightarrow C_2H_3+CHO+CHO$		7.83[+16]	−1.80		$k_{g83}=k_{g102}$
g84	$C_4H_4+H\rightleftarrows n\text{-}C_4H_5$		5.80[+12]	0.24	12.4	l
g85	$C_4H_4\rightleftarrows C_2H_2+C_2H_2$	10 Torr	7.91[+54]	−12.27	408.8	m
		20 Torr	1.33[+53]	−11.68	407.2	m
		50 Torr	3.31[+50]	−10.83	404.1	m
g86	$C_2H_2+C_2H_3\rightleftarrows C_4H_4+H$		1.70[+12]		20.4	72
g87	$C_3H_2+{}^{(1)}CH_2\rightleftarrows C_4H_4$		2.00[+13]			estimated
g88	$C_3H_2+{}^{(3)}CH_2\rightleftarrows C_4H_4$		2.00[+12]			estimated
g89	$C_3H_3+{}^{(1)}CH_2\rightleftarrows C_4H_4+H$		2.00[+13]			estimated
g90	$C_3H_3+{}^{(3)}CH_2\rightleftarrows C_4H_4+H$		2.00[+12]			estimated
g91	$C_4H_4+H\rightleftarrows n\text{-}C_4H_3+H_2$		3.16[+11]	0.70	33.5	$k_{g91}=k_{g37}$
g92	$C_4H_4+H\rightleftarrows i\text{-}C_4H_3+H_2$		3.16[+11]	0.70	33.5	$k_{g92}=k_{g37}$
g93	$C_4H_4+OH\rightleftarrows n\text{-}C_4H_3+H_2O$		2.20[+13]		17.5	75
g94	$C_4H_4+OH\rightleftarrows i\text{-}C_4H_3+H_2O$		2.20[+13]		17.5	75
g95	$C_4H_4\rightleftarrows C_4H_2+H_2$	10 Torr	3.39[+54]	−12.27	408.8	m
		20 Torr	5.70[+52]	−11.68	407.2	m
		50 Torr	1.42[+50]	−10.83	404.1	m
g96	$n\text{-}C_4H_3+H+M\rightleftarrows C_4H_4+M$		1.00[+15]			62
g97	$i\text{-}C_4H_3+H+M\rightleftarrows C_4H_4+M$		1.00[+15]			$k_{g97}=k_{g96}$
g98	$C_2H_2+C_2H+M\rightleftarrows n\text{-}C_4H_3+M$		1.00[+16]			n
g99	$n\text{-}C_4H_3+H\rightleftarrows C_4H_2+H_2$		1.50[+15]			$k_{g99}=k_{g42}/2$
g100	$i\text{-}C_4H_3+H\rightleftarrows C_4H_2+H_2$		3.00[+15]			$k_{g100}=k_{g42}$
g101	$n\text{-}C_4H_3+O_2\rightarrow C_2H+CHO+CHO$		7.83[+16]	−1.8		$k_{g101}=k_{g102}$
g102	$i\text{-}C_4H_3+O_2\rightarrow C_2H+CH_2O+CO$		7.83[+16]	−1.8		77
g103	$C_4H_2+H+M\rightleftarrows n\text{-}C_4H_3+M$		1.52[+18]	−0.52	113.8	o
g104	$C_4H_2+H+M\rightleftarrows i\text{-}C_4H_3+M$		1.52[+18]	−0.52	113.8	$k_{g104}=k_{g103}$
g105	$C_2H_2+C_2H\rightleftarrows C_4H_2+H$		4.00[+13]			62
g106	$C_4H+H_2\rightleftarrows C_4H_2+H$		8.00[+12]		11.0	$k_{g106}=k_{g46}$
g107	$C_4H_2+OH\rightleftarrows C_3H_2+CHO$		6.66[+12]		−1.7	59
	Formation and reactions of C_6H_x species					
g108	$n\text{-}C_6H_7+H\rightleftarrows C_6H_6+H_2$		1.50[+13]			$k_{g108}=k_{g42}/2$
g109	$n\text{-}C_6H_7+O_2\rightarrow n\text{-}C_4H_5+CHO+CHO$		7.83[+16]	−1.80		$k_{g109}=k_{g102}$
g110	$C_6H_6+H\rightleftarrows n\text{-}C_6H_7$		5.80[+12]	0.24	12.4	$k_{g110}=k_{g84}$
g111	$n\text{-}C_4H_5+C_2H_2\rightleftarrows C_6H_6+H$		7.13[−01]	3.48	38.0	p, 10–50 Torr
g112	$C_3H_3+C_3H_3\rightleftarrows C_6H_6$		2.00[+11]			estimated
g113	$C_6H_6+H\rightleftarrows n\text{-}C_6H_5+H_2$		3.16[+11]	0.70	33.5	$k_{g113}=k_{g37}$
g114	$C_6H_6+OH\rightleftarrows n\text{-}C_6H_5+H_2O$		2.20[+13]		17.5	$k_{g114}=k_{g93}$
g115	$n\text{-}C_6H_5+O_2\rightarrow n\text{-}C_4H_3+CHO+CHO$		7.83[+16]	−1.80		$k_{g115}=k_{g102}$
g116	$n\text{-}C_6H_5+H\rightleftarrows C_6H_4+H_2$		1.50[+13]			$k_{g116}=k_{g42}/2$
g117	$C_6H_4+H\rightleftarrows n\text{-}C_6H_5$		5.80[+12]	0.24	12.4	$k_{g117}=k_{g84}$
g118	$C_4H_2+C_2H_3\rightleftarrows C_6H_4+H$		1.70[+12]		20.4	$k_{g118}=k_{g86}$
g119	$n\text{-}C_4H_3+C_2H_2\rightleftarrows C_6H_4+H$	10 Torr	2.03[+23]	−3.13	84.1	p
		20 Torr	7.55[+20]	−2.44	79.3	p
		50 Torr	4.71[+17]	−1.52	72.7	p
g120	$C_6H_4+H\rightleftarrows n\text{-}C_6H_3+H_2$		3.16[+11]	0.70	33.5	$k_{g120}=k_{g37}$
g121	$C_6H_4+OH\rightleftarrows n\text{-}C_6H_3+H_2O$		2.20[+13]		17.5	$k_{g121}=k_{g93}$
g122	$n\text{-}C_6H_3+H+M\rightleftarrows C_6H_4+M$		1.00[+15]			$k_{g122}=k_{g96}$
g123	$C_4H_2+C_2H+M\rightleftarrows n\text{-}C_6H_3+M$		1.00[+16]			$k_{g123}=k_{g98}$
g124	$n\text{-}C_6H_3+O_2\rightarrow C_4H+CHO+CHO$		7.83[+16]	−1.80		$k_{g124}=k_{g102}$
g125	$n\text{-}C_6H_3+H\rightleftarrows C_6H_2+H_2$		1.50[+13]			$k_{g125}=k_{g42}/2$

TABLE I. (*Continued*).

No.	Reaction[a]		Forward rate coefficient[b] A	n	E	References and/or comments
g126	$C_6H_2+H+M \rightleftarrows n\text{-}C_6H_3+M$		1.52[+18]	−0.52	113.8	$k_{g126}=k_{g103}$
g127	$C_4H_2+C_2H \rightleftarrows C_6H_2+H$		4.00[+13]			$k_{g127}=k_{g105}$
g128	$C_2H_2+C_4H \rightleftarrows C_6H_2+H$		4.00[+13]			$k_{g128}=k_{g105}$
g129	$C_6H+H_2 \rightleftarrows C_6H_2+H$		8.00[+12]		11.0	$k_{g129}=k_{g46}$
	Formation and reactions of one-ring aromatics					
g130	$n\text{-}C_4H_3+C_2H_2 \rightleftarrows A_1^-$	10 Torr	1.32[+51]	−11.79	90.4	p
		20 Torr	2.48[+48]	−10.94	86.4	p
		50 Torr	3.92[+44]	−9.77	80.5	p
g131	$n\text{-}C_6H_5 \rightleftarrows A_1^-$	10 Torr	6.04[+62]	−15.74	104.7	q
		20 Torr	2.93[+60]	−14.99	102.0	q
		50 Torr	6.87[+56]	−13.84	97.0	q
g132	$n\text{-}C_4H_5+C_2H_2 \rightleftarrows A_1+H$		2.48[+13]	−0.33	23.4	p, 10–50 Torr
g133	$n\text{-}C_6H_7 \rightleftarrows A_1+H$		6.04[+62]	−15.74	104.7	$k_{g133}=k_{g131}$
			2.93[+60]	−14.99	102.0	$k_{g133}=k_{g131}$
			6.87[+56]	−13.84	97.0	$k_{g133}=k_{g131}$
g134	$A_1+H \rightleftarrows A_1^-+H_2$		2.50[+14]		66.9	80
g135	$A_1+OH \rightleftarrows A_1^-+H_2O$		2.10[+13]		19.1	81
g136	$A_1^-+H \rightleftarrows A_1$	10 Torr	5.45[+42]	−8.74	61.6	r
		20 Torr	3.48[+39]	−7.77	55.9	r
		50 Torr	2.18[+35]	−6.51	48.2	r
g137	$A_1+OH \rightarrow CH_2O+C_2H_2+C_3H_3$		1.00[+12]			estimated
g138	$A_1^-+O_2 \rightarrow n\text{-}C_4H_5+CO+CO$		2.00[+12]		31.3	83
g139	$A_1^-+C_2H_2 \rightleftarrows A_1C_2H+H$		4.00[+13]		42.3	72
g140	$n\text{-}C_4H_3+C_4H_2 \rightleftarrows A_1C_2H^-$	10 Torr	1.32[+51]	−11.79	90.4	$k_{g140}=k_{g130}$
		20 Torr	2.48[+48]	−10.94	86.4	$k_{g140}=k_{g130}$
		50 Torr	3.92[+44]	−9.77	80.5	$k_{g140}=k_{g130}$
g141	$A_1C_2H+H \rightleftarrows A_1C_2H^-+H_2$		2.50[+14]		66.9	$k_{g141}=k_{g134}$
g142	$A_1C_2H+OH \rightleftarrows A_1C_2H^-+H_2O$		2.10[+13]		19.1	$k_{g142}=k_{g135}$
g143	$A_1C_2H^-+H \rightleftarrows A_1C_2H$	10 Torr	5.45[+42]	−8.74	61.6	$k_{g143}=k_{g136}$
		20 Torr	3.48[+39]	−7.77	55.9	$k_{g143}=k_{g136}$
		50 Torr	2.18[+35]	−6.51	48.2	$k_{g143}=k_{g136}$
g144	$A_1C_2H^-+O_2 \rightarrow C_6H_4+CHO+CO$		2.00[+12]		31.3	$k_{g151}=k_{g138}$
g145	$n\text{-}C_6H_3+C_2H_2 \rightleftarrows A_1C_2H^*$	10 Torr	1.32[+51]	−11.79	90.4	$k_{g145}=k_{g130}$
		20 Torr	2.48[+48]	−10.94	86.4	$k_{g145}=k_{g130}$
		50 Torr	3.92[+44]	−9.77	80.5	$k_{g145}=k_{g130}$
g146	$A_1C_2H+H \rightleftarrows A_1C_2H^*+H_2$		2.50[+14]		66.9	$k_{g146}=k_{g134}$
g147	$A_1C_2H+OH \rightleftarrows A_1C_2H^*+H_2O$		2.10[+13]		19.1	$k_{g147}=k_{g135}$
g148	$A_1C_2H^*+H \rightleftarrows A_1C_2H$	10 Torr	5.45[+42]	−8.74	61.6	$k_{g148}=k_{g136}$
		20 Torr	3.48[+39]	−7.77	55.9	$k_{g148}=k_{g136}$
		50 Torr	2.18[+35]	−6.51	48.2	$k_{g148}=k_{g136}$
g149	$A_1C_2H^*+O_2 \rightarrow C_6H_4+CHO+CO$		2.00[+12]		31.3	$k_{g149}=k_{g138}$
g150	$A_1C_2H+OH \rightarrow A_1+CHCO$		1.00[+12]			estimated
	Formation and reactions of two-ring aromatics					
g151	$A_1C_2H^*+C_2H_2 \rightleftarrows A_2^-X$		4.00[+13]		42.3	$k_{g151}=k_{g139}$
g152	$A_2+H \rightleftarrows A_2^-X+H_2$		2.50[+14]		66.9	$k_{g152}=k_{g134}$
g153	$A_2+OH \rightleftarrows A_2^-X+H_2O$		2.10[+13]		19.1	$k_{g153}=k_{g135}$
g154	$A_2^-X+H \rightleftarrows A_2$	10 Torr	5.45[+42]	−8.74	61.6	$k_{g154}=k_{g136}$
		20 Torr	3.48[+39]	−7.77	55.9	$k_{g154}=k_{g136}$
		50 Torr	2.18[+35]	−6.51	48.2	$k_{g154}=k_{g136}$
g155	$A_2^-X+O_2 \rightarrow A_1C_2H+CHO+CO$		2.00[+12]		31.3	$k_{g155}=k_{g138}$
g156	$A_2+OH \rightarrow A_1C_2H+CHO+{}^{(3)}CH_2$		1.00[+12]			estimated
g157	$A_2^-X+C_2H_2 \rightleftarrows A_2R_5+H$		4.00[+13]		42.3	$k_{g157}=k_{g139}$
g158	$A_2R_5+OH \rightarrow A_2+CHCO$		1.00[+12]			estimated

[a]Reactions with the sign "$\rightleftarrows$" were treated as reversible and those with "$\rightarrow$" as irreversible.

[b]The forward rate coefficient $k = AT^n\exp(-E/RT)$; the units are cm^3, K, kJ, mol, and s. The rate coefficients for the reverse direc-

TABLE I. (*Continued*).

tion were determined via equilibrium constants. Numbers in square brackets denote powers of 10.
[c]The rate coefficient expression is obtained using the Troe-Golden formalism (Refs. 84–86) in the format reported in Ref. 18 and using the data reported in Refs. 40 and 41.
[d]The rate coefficient expression is obtained using the Troe-Golden formalism (Refs. 84–86) in the format reported in Ref. 18 and using the data reported in Refs. 40 and 50; this expression is valid for a pressure range of 10 to 50 Torr.
[e]The rate coefficient expression is obtained using the Troe-Golden formalism (Refs. 84–86) in the format reported in Ref. 18 and using the data reported in Refs. 40 and 51.
[f]The rate coefficient expression is obtained using the Troe-Golden formalism (Refs. 84–86) in the format reported in Ref. 18 and using the data reported in Ref. 53.
[g]The rate coefficient expression is obtained by fitting the data of Refs. 56 and 57.
[h]The rate coefficient expression is obtained from the rate coefficient of the reverse reaction, and the latter was calculated using a computer code of Gilbert and Smith (Ref. 87) with the transition state parameters of Ref. 61.
[i]The total rate coefficient value for reactions ($g47$) and ($g48$) is taken from Ref. 63 and the branching ratio is from Ref. 64.
[j]The rate coefficient is estimated based on the value of 6.0×10^{12} for $M=N_2$ suggested in Ref. 68 and the relative collision efficiency $\beta_{H_2}/\beta_{N_2}=2.5$ from Ref. 35.
[k]The rate coefficient used by Lutz *et al.* (Ref. 59) is multiplied by a factor of 2, following the results of Ref. 33.
[l]Obtained from the rate coefficient of the reverse reaction given in Ref. 73 and the equilibrium constant.
[m]The rate coefficient expression is calculated using a computer code of Gilbert and Smith (Ref. 87) with the transition state parameters of Ref. 74. The branching ratio for reaction channels ($g85$) and ($g95$) is 0.7/0.3.
[n]Derived from the data given by Duran *et al.* (Ref. 76).
[o]Obtained from the rate coefficient for the reverse reaction reported (Ref. 62) and the equilibrium constant.
[p]The rate coefficient expression is obtained using the *QRRK* computer code and the parameters of Ref. 78.
[q]The rate coefficient expression is calculated using a computer code of Gilbert and Smith (Ref. 87) with the transition state parameters of Ref. 79.
[r]The rate coefficient expression is calculated using a computer code of Gilbert and Smith (Ref. 87) with the transition state parameters of Ref. 82.

TABLE II. Nomenclature of selected species in Tables I and III.

Name used	Structure	Name used	Structure
n-C_4H_{10}	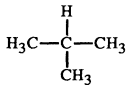	t-C_4H_9	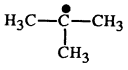
n-C_4H_3	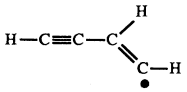	i-C_4H_3	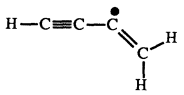
n-C_4H_5	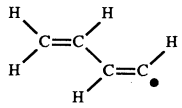	n-C_6H_5	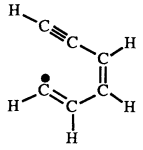
n-C_6H_7	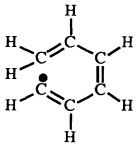	A_1	
A_1^-		A_1C_2H	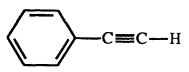
$A_1C_2H^*$	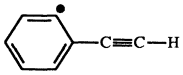	$A_1C_2H_2$	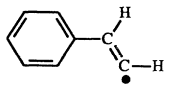
A_2^-X	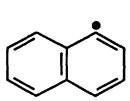	A_2R_5	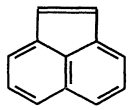

dynamic data for the calculation of the equilibrium constants were taken from the following sources: for most of the small molecules from the compilation of Burcat,[90] for HO_2 from the Sandia compilation,[91] for C_2H and the related C_t-H group additivity from the recent results of Green *et al.*,[92] and for C_2H_3, C_4H_2 and larger hydrocarbons from Stein and Fahr.[93]

C. Surface reaction mechanism

The surface processes were modeled in terms of elementary chemical reactions of surface sites. These reactions and associated rate parameters were founded on the premise that chemical reactivity of solid carbonaceous materials is localized on the carbon sites in a manner similar to that of the corresponding gaseous species. In other words, the kinetics of analogous elementary chemical reactions on a per site basis is the same for all forms of carbon.[18,94,95] Following this assumption, specific surface reactions were postulated. A complete list of these reactions, comprising the surface reaction mechanism adopted for the present study, is given in Table III. Most reactions of the surface reaction mechanism were founded on analogous gas-phase reactions. For the purpose of estimation of the rate parameters for these surface reactions, most closely related prototype gas-phase reactions were chosen; the latter are also listed in Table III.

The nomenclature for the gaseous chemical species appearing in Table III is the same as the one used for the gas-phase reaction mechanism discussed in Sec. II B above. The surface sites, or "surface species," are defined as follows. "C_d" denotes an sp^3 carbon radical site and "C_dR" an "R" bonded to this site. Similarly, "C_g" denotes an sp^2 carbon radical site and "C_gR" an R bonded to this site. The "C_dH" sites signify hydrogenated diamond surface sites and "C_gH" hydrogenated nondiamond surface sites. The rest of the "C_dR" and "C_gR" sites represent hydrocarbon surface intermediates or "complexes." For instance, species C_gC_2H, $C_gC_2H^*$, and $C_gC_2H_2$ appearing in Table III are surface analogs of gas-phase species A_1C_2H, $A_1C_2H^*$, and $A_1C_2H_2$ described in Table II, respectively. At the present level of modeling, we do not distinguish among various forms of nondiamond materials—they all are lumped into the C_g-type surface sites. Their general nature, nonetheless, could be often revealed upon the identification and analysis of reactions responsible for the formation of these sites at a given set of initial conditions. Our model calculates two-dimensional concentrations of surface sites and the linear rate of carbon deposition in a manner which will be described in Sec. II D below.

The reaction mechanism of Table III includes a detailed description of the following processes occurring on diamond (111) surface: surface site activation by the abstraction of the terminal H atoms leading to the formation of surface radicals; deactivation of the surface radical sites by the abstraction of H atoms from gaseous species and by recombination with free gaseous atoms and radicals; growth of diamond by the addition of methyl, acetylene,[26] and other C_2H_X species—vinyl, ethylene, ethyl, and ethane; condensation of aromatic species on the growing surface, thereby covering diamond sp^3 sites with nondiamond sp^2 sites;[18] growth of the sp^2 sites by the acetylene-addition mechanism;[95,98] gasification of sp^2 carbon via reactions with hydrogen atoms, hydroxyl radicals, oxygen atoms, and oxygen molecules; and interconversion of sp^2 and sp^3 sites into one another.

The rates of the gas-surface reactions, the most common reaction type in the surface reaction mechanism, were formulated based on equation

$$\frac{r_s}{\nu_s}=\frac{r_g}{\nu_g}=\gamma\ , \tag{1}$$

which expresses the assumption of equal reaction probabilities for similar gas-phase and gas-surface reactions. Here r_s is the rate of the gas-surface reaction per surface site, ν_s is the rate of collisions between a given gaseous species and a given surface site, r_g and ν_g are the corresponding properties of the prototype gas-phase reaction, and γ is the probability of a given reaction upon collision. The gas-phase rates are given as[100]

$$r_g=k_gC_g \tag{2}$$

and

$$\nu_g=\left[\frac{8\kappa_BT_g}{\pi\mu_g}\right]^{1/2}\sigma_gC_g\ , \tag{3}$$

where k_g is the per-molecule rate coefficient of the prototype gas-phase reaction, C_g is the concentration of the gas-phase reactant [e.g., the concentration of H atoms in reaction (*s*1)], κ_B is the Boltzmann constant, T_g is the gas temperature, μ_g is the reduced mass for the reactants of the prototype reaction, $\sigma_g=\frac{1}{4}\pi(d_g+d_p)^2$ is the collision cross section of the prototype reaction, and d_g and d_p are the diameters of the reactant and prototype gaseous species, respectively. The collision rate for the gas-surface reaction per surface site is defined as

$$\nu_s=\frac{1}{4}\bar{c}C_g\sigma_s=\frac{1}{4}\left[\frac{8\kappa_BT_g}{\pi m_g}\right]^{1/2}C_g\sigma_s\ , \tag{4}$$

which is the product of the collision frequency of the reacting gaseous series with unit area of the substrate[101] $\frac{1}{4}\bar{c}C_g$, and the collisional cross section of the surface site σ_s. Here $\bar{c}$ and m_g are the average velocity and molecular mass of the gaseous species attacking the surface. The value of σ_s assumed in the present study is 2.6 Å^2/site for both diamond sp^3 and nondiamond sp^2 surfaces.

Substituting Eqs. (2)–(4) into Eq. (1) and expressing for r_s, we obtain

$$r_s=\frac{\sigma_sk_g}{4\sigma_g\left[1+\frac{m_p}{m_g}\right]^{1/2}}C_g\ , \tag{5}$$

where m_p is the molecular mass of the prototype gaseous species. Equation (5) defines the per-site rate coefficient of the gas-surface reaction k_s,

TABLE III. Surface reaction mechanism. Numbers in square brackets denote powers of 10.

No.	Surface reaction[a]	Rate coefficient[b] A	n	E	x	Prototype gas-phase reaction[c]	Reference for k_g and/or comments
	Activation and deactivation of diamond surface						
s1	$C_dH + H \rightarrow C_d + H_2$	2.3[−12]		29.3	s	$i\text{-}C_4H_{10} + H \rightleftarrows t\text{-}C_4H_9 + H_2$	d
	$C_dH + H \leftarrow C_d + H_2$	2.5[−17]	1.12	62.5			
s2	$C_dH + OH \rightarrow C_d + H_2O$	2.3[−14]		−0.8	s	$i\text{-}C_4H_{10} + OH \rightleftarrows t\text{-}C_4H_9 + H_2O$	e
	$C_dH + OH \leftarrow C_d + H_2O$	1.6[−18]	1.12	95.8			
s3	$C_dH + CH_3 \rightarrow C_d + CH_4$	5.2[−16]		33.1	s	$i\text{-}C_4H_{10} + CH_3 \rightleftarrows t\text{-}C_4H_9 + CH_4$	f
	$C_dH + CH_3 \leftarrow C_d + CH_4$	2.8[−19]	1.09	71.7			
s4	$C_d + H \rightarrow C_dH$	5.2[−13]			s	$t\text{-}C_4H_9 + H \rightleftarrows i\text{-}C_4H_{10}$	g
	$C_d + H \leftarrow C_dH$	3.7[+15]	−0.72	399.5			
	Diamond growth by acetylene addition to C_d						
s5	$C_d + C_2H_2 \rightarrow C_dH + H$	1.3[−13]			s	$t\text{-}C_4H_9 + C_2H_2 \rightarrow$ products	$k_g = 1.7(-11)$, estimated
	Addition of methyl radicals						
s6	$C_d + CH_3 \rightarrow C_dCH_3$	1.3[−29]	4.72	−27.3	s	$t\text{-}C_4H_9 + CH_3 \rightleftarrows C(CH_3)_4$	h
	$C_d + CH_3 \leftarrow C_dCH_3$	1.5[+15]		351.5			
s7	$C_dCH_3 + H \rightarrow C_d + CH_4$	2.5[−06]	−1.33	109.7	s	$C_2H_6 + H \rightleftarrows CH_3 + CH_4$	i
	$C_dCH_3 + H \leftarrow C_d + CH_4$	1.3[−12]		167.4			
s8	$C_dCH_3 + H \rightarrow C_dCH_2 + H_2$	1.8[−23]	3.50	21.8	s	$C_2H_6 + H \rightleftarrows C_2H_5 + H_2$	35
	$C_dCH_3 + H \leftarrow C_dCH_2 + H_2$	3.5[−28]	4.30	45.0			
s9	$C_dCH_3 + OH \rightarrow C_dCH_2 + H_2O$	4.9[−19]	1.90	4.7	s	$C_2H_6 + OH \rightleftarrows C_2H_5 + H_2O$	52
	$C_dCH_3 + OH \leftarrow C_dCH_2 + H_2O$	2.5[−21]	2.31	89.3			
s10	$C_dCH_3 + CH_3 \rightarrow C_dCH_2 + CH_4$	9.4[−27]	4.00	34.7	s	$C_2H_6 + CH_3 \rightleftarrows C_2H_5 + CH_4$	35
	$C_dCH_3 + CH_3 \leftarrow C_dCH_2 + CH_4$	3.7[−28]	4.39	61.3			
s11	$C_dCH_2 + H \rightarrow C_dCH_3$	2.3[−08]	−0.95	13.7	s	$C_2H_5 + H \rightleftarrows C_2H_6$	40,51
	$C_dCH_2 + H \leftarrow C_dCH_3$	2.2[+18]	−0.97	425.2			
	Diamond growth via C_d-C_2H_y surface complexes						
s12	$C_dCH_2 + CH_3 \rightarrow C_dC_2H_5$	8.3[−12]	−0.50		s	$C_2H_5 + CH_3 \rightleftarrows C_3H_8$	68
	$C_dCH_2 + CH_3 \leftarrow C_dC_2H_5$	3.3[+21]	−2.06	365.0			
s13	$C_d + C_2H_5 \rightarrow C_dC_2H_5$	1.4[−13]			s	$C_2H_5 + C_2H_5 \rightleftarrows C_4H_{10}$	68
	$C_d + C_2H_5 \leftarrow C_dC_2H_5$	1.1[+22]	−2.25	351.5			
s14	$C_dC_2H_5 + H \rightarrow C_d + C_2H_6$	2.5[−06]	−1.33	109.7	s		$k_{s14} = k_{s7}$
	$C_dC_2H_5 + H \leftarrow C_d + C_2H_6$	1.3[−12]		167.4			
s15	$C_dC_2H_5 + H \rightarrow C_dCH_2 + CH_4$	2.5[−06]	−1.33	109.7	s		$k_{s15} = k_{s7}$
	$C_dC_2H_5 + H \leftarrow C_dCH_2 + CH_4$	1.3[−12]		167.4			
s16	$C_dC_2H_5 + H \rightarrow C_dC_2H_4 + H_2$	1.8[−23]	3.50	21.8	s		$k_{s16} = k_{s8}$
	$C_dC_2H_5 + H \leftarrow C_dC_2H_4 + H_2$	3.5[−28]	4.30	45.0			
s17	$C_dC_2H_5 + OH \rightarrow C_dC_2H_4 + H_2O$	4.9[−19]	1.90	4.7	s		$k_{s17} = k_{s9}$
	$C_dC_2H_5 + OH \leftarrow C_dC_2H_4 + H_2O$	2.5[−21]	2.31	89.3			

TABLE III. (*Continued*).

No.	Surface reaction[a]	Rate coefficient[b] A	n	E	x	Prototype gas-phase reaction[c]	Reference for k_g and/or comments
*s*18	$C_dC_2H_5+CH_3\rightarrow C_dC_2H_4+CH_4$	9.4[−27]	4.00	34.7	*s*		$k_{s18}=k_{s10}$
	$C_dC_2H_5+CH_3\leftarrow C_dC_2H_4+CH_4$	3.7[−28]	4.39	61.3			
*s*19	$C_dC_2H_4+H\rightarrow C_dC_2H_5$	2.3[−08]	−0.95	13.7	*s*		$k_{s19}=k_{s11}$
	$C_dC_2H_4+H\leftarrow C_dC_2H_5$	2.2[+18]	−0.97	425.2			
*s*20	$C_d+C_2H_4\rightarrow C_dC_2H_4$	4.4[−15]		32.2	*s*	$CH_3+C_2H_4\rightleftarrows C_3H_7$	68
	$C_d+C_2H_4\leftarrow C_dC_2H_4$	5.1[+15]	−1.50	133.7			
*s*21	$C_dC_2H_4\rightarrow C_dH+H$	1.0[+06]		60.0	*s*		j
*s*22	$C_dC_2H_4+H\rightarrow C_dC_2H_3+H_2$	1.0[−12]			*s*	$C_2H_5+H\rightleftarrows C_2H_4+H_2$	35
	$C_dC_2H_4+H\leftarrow C_dC_2H_3+H_2$	2.0[−13]	0.32	275.0			
*s*23	$C_d+C_2H_3\rightarrow C_dC_2H_3$	2.1[−13]			*s*	$C_2H_5+C_2H_3\rightleftarrows l\text{-}C_4H_8$	68
	$C_d+C_2H_3\leftarrow C_dC_2H_3$	3.1[+21]	−2.07	401.6			
*s*24	$C_dC_2H_3+H\rightarrow C_dC_2H_4$	4.8[−16]	0.87	−5.5	*s*	$C_2H_4+H\rightleftarrows C_2H_5$	k
	$C_dC_2H_3+H\leftarrow C_dC_2H_4$	1.1[+09]	0.73	154.2			
*s*25	$C_dC_2H_3+H\rightarrow C_d+C_2H_4$	2.7[−15]			*s*	$C_3H_6+H\rightleftarrows CH_3+C_2H_4$	$k_g=1.7(-13)$, estimated
	$C_dC_2H_3+H\leftarrow C_d+C_2H_4$	2.9[−21]	1.32	35.2			
*s*26	$C_dC_2H_3+H\rightarrow C_dH+H_2+H$	1.2[−14]	0.70	33.5	*s*	$C_2H_4+H\rightarrow C_2H_3+H_2$	55
*s*27	$C_dC_2H_3+OH\rightarrow C_dH+H_2O+H$	6.5[−13]		24.9	*s*	$C_2H_4+OH\rightarrow C_2H_3+H_2O$	Table I
*s*28	$C_dC_2H_3+CH_3\rightarrow C_dH+CH_4+H$	7.2[−14]		54.5	*s*	$C_2H_4+CH_3\rightarrow C_2H_3+CH_4$	35
	Diamond growth by acetylene addition to C_d-CH_2						
*s*29	$C_dCH_2+C_2H_2\rightarrow C_dH+H$	1.3[−13]			*s*		$k_{s29}=k_{s5}$
	Condensation of benzene						
*s*30	$A_1\rightarrow C_gH$	4.1[+01]	0.50		*g*		l
	Activation and deactivation of sp^2 carbon						
*s*31	$C_gH+H\rightarrow C_g+H_2$	6.3[−12]		66.9	*s*	$A_1+H\rightleftarrows A_1^-+H_2$	80
	$C_gH+H\leftarrow C_g+H_2$	1.2[−15]	0.53	38.1			
*s*32	$C_gH+OH\rightarrow C_g+H_2O$	4.0[−13]		19.1	*s*	$A_1+OH\rightleftarrows A_1^-+H_2O$	81
	$C_gH+OH\leftarrow C_g+H_2O$	4.7[−16]	0.53	53.7			
*s*33	$C_gH+CH_3\rightarrow C_g+CH_4$	1.0[−25]	3.70	39.7	*s*	$A_1+CH_3\rightleftarrows A_1^-+CH_4$	33
	$C_gH+CH_3\leftarrow C_g+CH_4$	9.5[−28]	4.21	16.3			
*s*34	$C_g+H\rightarrow C_gH$	4.6[−14]	0.68	3.6	*s*	$A_1^-+H\rightleftarrows A_1$	82
	$C_g+H\leftarrow C_gH$	1.8[+13]	0.55	465.1			
	Growth and gasification of sp^2 phase						
*s*35	$C_g+C_2H_2\rightarrow C_gC_2H_2$	1.3[−13]			*s*	$A_1^-+C_2H_2\rightleftarrows A_1C_2H_2$	98
	$C_g+C_2H_2\leftarrow C_gC_2H_2$	1.4[+17]	−1.34	199.6			
*s*36	$C_gC_2H_2+C_2H_2\rightarrow C_gH+H$	2.2[−20]	1.79	9.4	*s*	$A_1C_2H_2+C_2H_2\rightleftarrows A_2+H$	m
	$C_gC_2H_2+C_2H_2\leftarrow C_gH+H$	9.7[−11]	0.63	228.5			

TABLE III. (*Continued*).

No.	Surface reaction[a]	Rate coefficient[b] A	n	E	x	Prototype gas-phase reaction[c]	Reference for k_g and/or comments
*s*37	$C_gC_2H + H \rightarrow C_gC_2H_2$	1.4[−14]	0.32	8.5	*s*	$A_1C_2H + H \rightleftarrows A_1C_2H_2$	n
	$C_gC_2H + H \leftarrow C_9C_2H_2$	3.4[+08]	0.61	182.9			
*s*38	$C_gC_2H_2 + H \rightarrow C_gC_2H + H_2$	6.8[−13]			*s*	$A_1C_2H_2 + H \rightleftarrows A_1C_2H + H_2$	o
	$C_gC_2H_2 + H \leftarrow C_gC_2H + H_2$	2.3[−12]	0.11	258.3			
*s*39	$C_g + C_2H_2 \rightarrow C_gC_2H + H$	5.4[−13]		42.3	*s*	$A_1^- + C_2H_2 \rightleftarrows A_1C_2H + H$	72
	$C_g + C_2H_2 \leftarrow C_gC_2H + H$	4.0[−05]	−1.63	67.5			
*s*40	$C_gC_2H + H \rightarrow C_gC_2H^* + H_2$	6.3[−12]		66.9	*s*		$k_{s40} = k_{s31}$
	$C_gC_2H + H \leftarrow C_gC_2H^* + H_2$	1.2[−15]	0.53	38.1			
*s*41	$C_gC_2H + OH \rightarrow C_gC_2H^* + H_2O$	4.0[−13]		19.1	*s*		$k_{s41} = k_{s32}$
	$C_gC_2H + OH \leftarrow C_gC_2H^* + H_2O$	4.7[−16]	0.53	53.7			
*s*42	$C_gC_2H + CH_3 \rightarrow C_gC_2H^* + CH_4$	1.0[−25]	3.70	39.7	*s*		$k_{s42} = k_{s33}$
	$C_gC_2H + CH_3 \leftarrow C_gC_2H^*CH_4$	9.5[−28]	4.21	16.3			
*s*43	$C_gC_2H^* + H \rightarrow C_gC_2H$	4.6[−14]	0.68	3.6	*s*		$k_{s43} = k_{s34}$
	$C_gC_2H^* + H \leftarrow C_gC_2H$	1.8[+13]	0.55	465.1			
*s*44	$C_gC_2H^* + C_2H_2 \rightarrow C_g$	5.2[−20]	1.65	10.5	*s*	$A_1C_2H^* + C_2H_2 \rightleftarrows A_2^-X$	p
	$C_gC_2H^* + C_2H_2 \leftarrow C_g$	1.8[+12]	0.78	404.1			
	$sp^2 \leftrightarrow sp^3$						
*s*45	$H + C_gH \rightarrow C_d$	3.7[−13]		50.0	*s*	$C_2H_4 + H \rightleftarrows C_2H_5$	q
	$H + C_gH \leftarrow C_d$	1.5[+11]	0.08	257.7			
	Gasification of sp^2 phase by oxidation						
*s*46	$C_g + O_2 \rightarrow$ products	3.0[−14]		31.3	*s*	$A_1^- + O_2 \rightarrow$ products	83
*s*47	$C_gC_2H^* + O_2 \rightarrow C_g +$ products	3.0[−14]		31.3	*s*		$k_{s47} = k_{s46}$
*s*48	$C_gC_2H_2 + O_2 \rightarrow C_g +$ products	6.5[−14]		−1.0	*s*	$C_2H_3 + O_2 \rightarrow CHO + CH_2O$	60
*s*49	$C_gH + OH \rightarrow$ products	8.8[+02]	0.5		*g*		r
*s*50	$C_gH + O \rightarrow$ products	8.8[+02]	0.5		*g*		$k_{s50} = k_{s49}$
*s*51	$C_gC_2H + OH \rightarrow C_gH + CH_2CO$	8.8[+02]	0.5		*g*		$k_{s51} = k_{s49}$
*s*52	$C_gC_2H + O \rightarrow C_gH + CHCO$	8.8[+02]	0.5		*g*		$k_{s52} = k_{s49}$

[a]The first row for each reaction number specifies the rate coefficient of the forward direction and the next row, if given, specifies the rate coefficient of the reverse direction of this reaction.

[b]The surface reaction rate coefficient $k = AT_x^n \exp(-E/RT_x)$; the units of A are cm, molecule, and s; the unit of T is K; and the units of E are kJ/mol; T_g and T_s are the gas-phase and substrate temperatures, respectively.

[c]The rate coefficients of the gas-phase reactions are taken at the high-pressure limits whenever applicable.

[d]The rate coefficient of the gas-phase reaction is taken from Ref. 35 for reaction *tertiary* C—H + H⇄*tertiary* C· + H_2.

[e]The rate coefficient of the gas-phase reaction is taken from Ref. 35 for reaction *tertiary* C—H + OH⇄*tertiary* C· + H_2O.

[f]The rate coefficient of the gas-phase reaction is estimated based on the rate coefficient $k_g = 1.6 \times 10^{-13} \exp(-33.1/RT)$, recommended by Warnatz (Ref. 35) for the reaction i-$C_4H_{10} + CH_3 \rightleftarrows C_4H_9 + CH_4$, and assuming $k_{\text{primary}}/k_{\text{tertiary}} = \frac{1}{5}$.

[g]The gas-phase rate coefficient is that of the reaction i-$C_3H_7 + H \rightleftarrows C_3H_8$; it is computed from the rate coefficient of the reverse reaction recommended by Warnatz (Ref. 35) and the equilibrium constant.

TABLE III. (*Continued*).

[h]The rate coefficient of the reverse gas-phase reaction is taken from Bernfeld and Skinner (Ref. 96).
[i]The rate coefficient of the reverse gas-phase reaction is taken from Tabayashi and Bauer (Ref. 97).
[j]The rate coefficient of the surface reaction is estimated; the activation energy is assumed to be equal to the endothermicity of H-atom displacement.
[k]The rate coefficient of the reverse gas-phase reaction is taken from Stewart and Golden (Ref. 53).
[l]The deposition rate coefficient is calculated from $k_s=\frac{1}{4}\gamma(8\kappa_B T_g/\pi m_{A_1})^{1/2}$, where m_{A_1} is the molecular mass of benzene and γ is the sticking coefficient (assumed to be 0.1 in this study).
[m]The rate coefficient of the gas-phase reaction is that of the reaction $n\text{-}C_4H_5+C_2H_2 \rightleftarrows A_1+H$, taken from Ref. 78.
[n]The rate coefficient of the gas-phase reaction is one half that of the reaction $C_2H_2+H \rightleftarrows C_2H_3$; the latter is taken from Ref. 61.
[o]The rate coefficient of the gas-phase reaction is that of the reaction $C_2H_3+H \rightleftarrows C_2H_2+H_2$, taken from Ref. 58.
[p]The rate coefficient of the gas-phase reaction is that of the reaction $n\text{-}C_4H_3+C_2H_2 \rightleftarrows A_1^-$, taken from Ref. 78.
[q]The rate coefficient of the forward surface reaction is estimated. Its reverse rate coefficient is calculated via the equilibrium constant of the gas-phase reaction listed, increasing the activation energy by 50 kJ/mol.
[r]The rate coefficient of the surface reaction is estimated as the frequency of collisions of OH radicals with the substrate surface multiplied by the reaction probability equal to 0.2, as determined for the oxidation of soot particles by OH in Ref. 99.

$$k_s=\frac{\sigma_s}{4\sigma_g\left[1+\frac{m_p}{m_g}\right]^{1/2}}k_g \ . \tag{6}$$

The rates of several gas-surface reactions, those describing gasification of the sp^2 carbon by OH radicals [reactions ($s49$) and ($s51$)], were estimated differently. Instead of relying on analogous gas-phase reactions, which are not well established, the rates of these reactions were expressed using the reaction probability γ, taking it to be equal to 0.2, following the results of Neoh *et al.*[99] for the oxidation of soot, i.e.,

$$r_s'=\gamma\nu_s' \ , \tag{7}$$

where r_s' and ν_s' are the gas-surface reaction and collision rates, respectively, per unit area. This leads to the definition of an equivalent, per unit area, rate coefficient expression

$$k_s'=\tfrac{1}{4}\gamma\bar{c}=0.05\left[\frac{8\kappa_B T_g}{\pi m_{\mathrm{OH}}}\right]^{1/2} . \tag{8}$$

The rates of reactions describing gasification of the sp^2 carbon by O atoms [reactions ($s50$) and ($s52$)] were assumed to be equal to those of OH radicals.

The rate of surface condensation of aromatic species [reaction ($s30$) in Table III] was estimated in a similar manner, using Eqs. (7) and (8), and considering γ to be the sticking probability. We envision that the surface condensation can proceed by several reaction mechanisms: by the formation of a chemical bond (chemisorption) upon collision of an aromatic species with an active surface site or by the initial formation of weak van der Waals bonds with sp^3 and sp^2 sites present on the surface (physisorption) followed by a rapid chemical transformation of the admolecule via its molecular decomposition or by its reaction with a gaseous species. It is also possible that coadsorption-induced condensation of aromatics on the growing surface can play a role. Some of these phenomena have been observed for benzene condensation on hot metal surfaces.[102] No information is available for condensation of aromatics on diamond surfaces. We assumed for the present work the sticking probability γ to be equal to 0.1. Sensitivity analysis performed during our study and discussed in Sec. III C below indicated that γ may be substantially lower than 0.1. Choosing a larger value $\gamma=0.1$ helped in the illustration and emphasis of the phenomena discussed.

The rates of unimolecular surface reactions [e.g., the reverse of reaction ($s4$)] were estimated via the detailed balancing and assuming that the equilibrium constants of the surface reactions are equal to those of the corresponding prototype gaseous reactions. The values of the rate coefficients for all surface reactions were fitted into the modified Arrhenius form over the temperature range of 500 to 1800 K, and the obtained parameters are listed in Table III.

D. Surface kinetics

Based on the formalism of the per-site rate coefficients developed above, the kinetics of the surface reactions is

treated in a manner similar to that of the gas-phase reactions, except that the concentration variables of the differential equations are now two-dimensional number densities of surface sites. That is, the reaction rates are given by

$$R_s = k_s C_g \chi_s \tag{9}$$

for gas-surface reactions and by

$$R_s = k_s \chi_s \tag{10}$$

for unimolecular surface reactions. χ_s denotes the number density of given surface sites per unit surface area. Equation (9) applies to all the reactions of Table III, except for $(s49)$–$(s52)$. The rate coefficients listed in Table III for the latter reactions are per unit area and hence their reaction rates are given as

$$R_s = k_s' C_g f \ , \tag{11}$$

where f is the fraction of the surface covered by the sp^2 sites. The formation-disappearance rate of a given surface species is expressed by

$$\frac{d\chi_i}{dt} = \sum_j \nu_{i,j} \alpha_{i,j} R_{s,j} \ , \tag{12}$$

where t is the reaction time, χ_i is the number density of the ith surface species, $\nu_{i,j}$ is the stoichiometric coefficient of the ith species in the jth reaction, and $\alpha_{i,j}$ is a factor that takes into account that the surface site density is changed when a transformation between the sp^3 and sp^2 carbon atoms occurs. This effect, however, is relatively small, about 5%—the density of carbon sites on (111) diamond surface is 0.363 Å^{-2} versus 0.382 Å^{-2} of the graphite surface. Therefore this difference is ignored in the present work, i.e., the value of α is assumed to be unity for all reactions.

The growth of the film was modeled using the technique of linear lumping. In this method, an infinite number of differential equations describing a polymerization-type process is lumped into a small number of differential equations for the moments of the polymer distribution function.[103–105] To illustrate the application of this technique to film growth, let us consider the following example. A film is deposited epitaxially by the following set of reactions:

$$\rightarrow C_{(1)}\text{—}H + H \rightleftarrows \rightarrow C_{(1)}\cdot + H_2 \ ,$$

$$\rightarrow C_{(1)}\cdot + C_2H_2 \rightarrow \rightarrow C_{(2)}\text{—}H \ ,$$

$$\rightarrow C_{(2)}\text{—}H + H \rightleftarrows \rightarrow C_{(2)}\cdot H_2 \ ,$$

$$\rightarrow C_{(2)}\cdot + C_2H_2 \rightarrow \rightarrow C_{(3)}\text{—}H \ ,$$

etc., where the subscript of $\rightarrow$C counts the depositing atomic carbon layers, from unity to infinity. The kinetic features of this infinite number of reactions (an infinite number of cycles, each consisting of the chemically similar two-stage process) can be represented by the kinetic properties of the lumped reaction system

$$\rightarrow C\text{—}H + H \rightleftarrows \rightarrow C\cdot + H_2 \ , \tag{13}$$

$$\rightarrow C\cdot + C_2H_2 \rightarrow \rightarrow C\text{—}H \ , \tag{14}$$

where $\rightarrow$C—H and $\rightarrow$C$\cdot$ represent lumped species, defined as

$$\chi_{\rightarrow C\text{—}H} = \sum_{i=1}^{\infty} \chi_{\rightarrow C_{(i)}\text{—}H} \tag{15}$$

and

$$\chi_{\rightarrow C\cdot} = \sum_{i=1}^{\infty} \chi_{\rightarrow C_{(i)}\cdot} \ , \tag{16}$$

respectively. Note that the number density of $\rightarrow$C—H sites does not change, in accordance with the epitaxial growth assumed in this example. The deposition rate—the number of carbon atoms deposited per unit area per unit time—is specified by the rate of reaction (14). Dividing this rate by the site number density of a complete layer determines the linear rate of the film growth.

Reactions $(s5)$, $(s21)$, and $(s26)$—$(s29)$ in Table III express this type of lumping for the growth of the sp^3 carbon and reaction $(s36)$ and $(s44)$ for the growth of the sp^2 carbon. The former are assumed irreversible, as required for the exact lumping.[104] This assumption is founded on the premise that the rate of the reverse reaction in these cases is negligible compared to the forward rate. Quantum-chemical calculations[26] indicate that, indeed, the last reaction step of the addition of an acetylene molecule to a diamond surface radical proceeds not only without activation energy but essentially irreversibly within the temperature range of diamond deposition. Since details of reactions $(s26)$–$(s29)$ and $(s21)$ are not fully understood, we assumed, by analogy, that these reaction steps are irreversible.

The linear growth rate of the carbonaceous film was defined in the present work as

$$\begin{aligned} 0.36\Delta h\, 2.6\times 10^{-16}(&2\mathcal{R}_{s5}+2\mathcal{R}_{s21}+2\mathcal{R}_{s26}+2\mathcal{R}_{s27}+2\mathcal{R}_{s28}+3\mathcal{R}_{s29}+6\mathcal{R}_{s30} \\ &+2\mathcal{R}_{s35}+2\mathcal{R}_{s36}+2\mathcal{R}_{s39}+2\mathcal{R}_{s44}-2\mathcal{R}_{s46}-2\mathcal{R}_{s47} \\ &-2\mathcal{R}_{s48}-2\mathcal{R}_{s49}-2\mathcal{R}_{s50}-2\mathcal{R}_{s51}-2\mathcal{R}_{s52})\ \mu\text{m/h} \ , \end{aligned} \tag{17}$$

where the $\mathcal{R}$'s are the net reaction rates and their integer multipliers are the numbers of carbon atoms incorporated into or removed from the film as a result of the corresponding lumping reaction sequences and Δh is the average interlayer distance in angstroms. The latter was defined as

$$\Delta h = 3.35f + 2.06(1-f) \ , \tag{18}$$

where 3.35 and 2.06 are the interlayer distances in graphite and diamond, respectively, and f, as defined earlier, is

the fraction of the surface covered by the sp^2 phase.

Surface condensation of aromatics presents a special case. First, the concentrations of large aromatic species were computed to be much smaller than that of benzene, and therefore, only condensation of benzene was considered in the present model. Second, we assumed that a benzene molecule depositing on the growing surface covers $6\times(1-f)$ sp^3 sites and $6\times f$ sp^2 sites. Similarly, the gasification of the sp^2 carbon uncovers $(1-f)$ sp^3 sites per each carbon atom removed from the surface.

III. RESULTS AND DISCUSSION

A. Test of the gas-phase model

The model predictions for the concentration profiles of the gaseous species were compared to the experimental data of Harris *et al.*[27] In the initial computations, using only the post-filament part ($x \geq 0$) of the temperature profile shown in Fig. 1, the computed concentration of acetylene was about two orders of magnitude below the measurements. Adding a pre-filament part symmetrically to the post-filament temperature profile brought the numbers closer together, but still by a factor of 6 different from each other. The agreement could be improved either by increasing the filament temperature or by assuming that the gas spends a finite period of time in the "filament zone." The latter, more plausible possibility was adopted in our model. The length of the filament zone was used to fine tune the model to reproduce the experimental data. The best-fit results were obtained with the filament-zone length of 1.5 cm (this length is the one shown in Fig. 1). These results along with several sensitivity tests are depicted in Fig. 2. The high sensitivity of acetylene concentration on the filament-zone length demonstrated in Fig. 2 indicates that the quantitive prediction of the gas-phase environment in the film deposition zone depends critically on the precise knowledge of the gas history in the filament zone.

B. Numerical predictions of the model

Concentration profiles of the most abundant among gaseous C_1H_x and C_2H_y species and that of benzene computed for the base case are shown in Fig. 3. Qualitatively, these results are very similar to those computed for comparable conditions but without considering transport phenomena (cf. Fig. 1 of Ref. 18). The most noticeable difference between the two sets of profiles is that in the present computation the methane concentration does not decrease with distance from the filament and the concentration of methyl radicals is much closer to that of acetylene molecules.

Figure 4 present the linear film growth rate and film quality computed as a function of substrate temperature and concentration of methane in the inlet mixture. The film quality is defined in the present work as the fraction of sp^2 carbon sites on the growing surface, meaning the lower the sp^2 fraction the higher the film quality. Every computer run started with the deposition on (111) diamond plane, assuming the substrate surface has microscopic steps.[95] The computations showed a period of

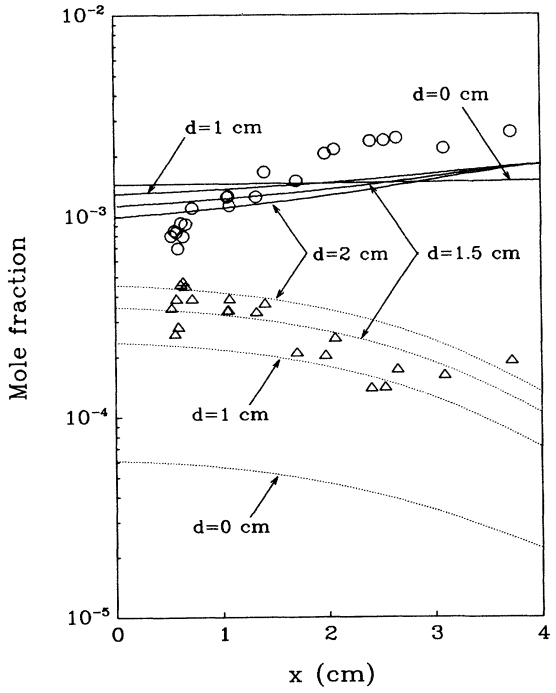

FIG. 2. Comparison of the model predictions (methane, solid lines; acetylene, dotted lines) to the experimental data of Harris *et al.* (Ref. 27) concentrations of methane (circles) and acetylene (triangles), at several values of the filament-zone length *d*.

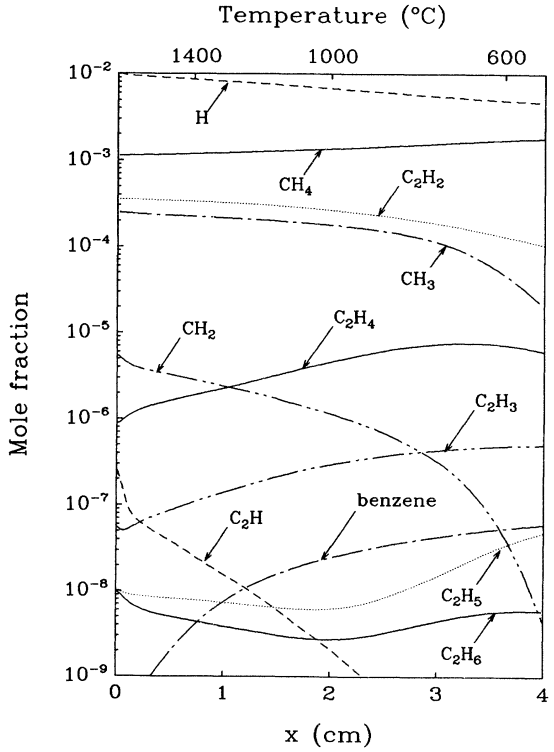

FIG. 3. Concentration profiles of selected species computed for the "base" case, a (0.3 vol % CH_4)-H_2 mixture at a pressure of 20 Torr.

nonsteady development and then approached a steady state. The duration of the nonsteady behavior is decreased with temperature: from about 1 h at 400 °C to about 0.1 s at 1400 °C. Figures 4(a) and 4(b), as well as in the rest of the figures, depict the steady-state results. An inspection of Fig. 4 indicates that our model predicts correctly experimental observations: the bell-shaped dependence of the growth rate and film quality on substrate temperature,[12,106–111] the decline in the film quality with the increase in the methane concentration,[5,12,109,112] the right order of magnitude of the deposition rate in hot-filament reactors,[27,111,113,114] the temperature of the peak deposition rate,[12,106–111] and its shifting to higher temperatures with the increase in methane concentration.[12,109] Our model predicts that when compared at the same substrate temperature, the deposition rate first increases with the increase in the initial methane concentration, reaches a maximum, and then slowly de-

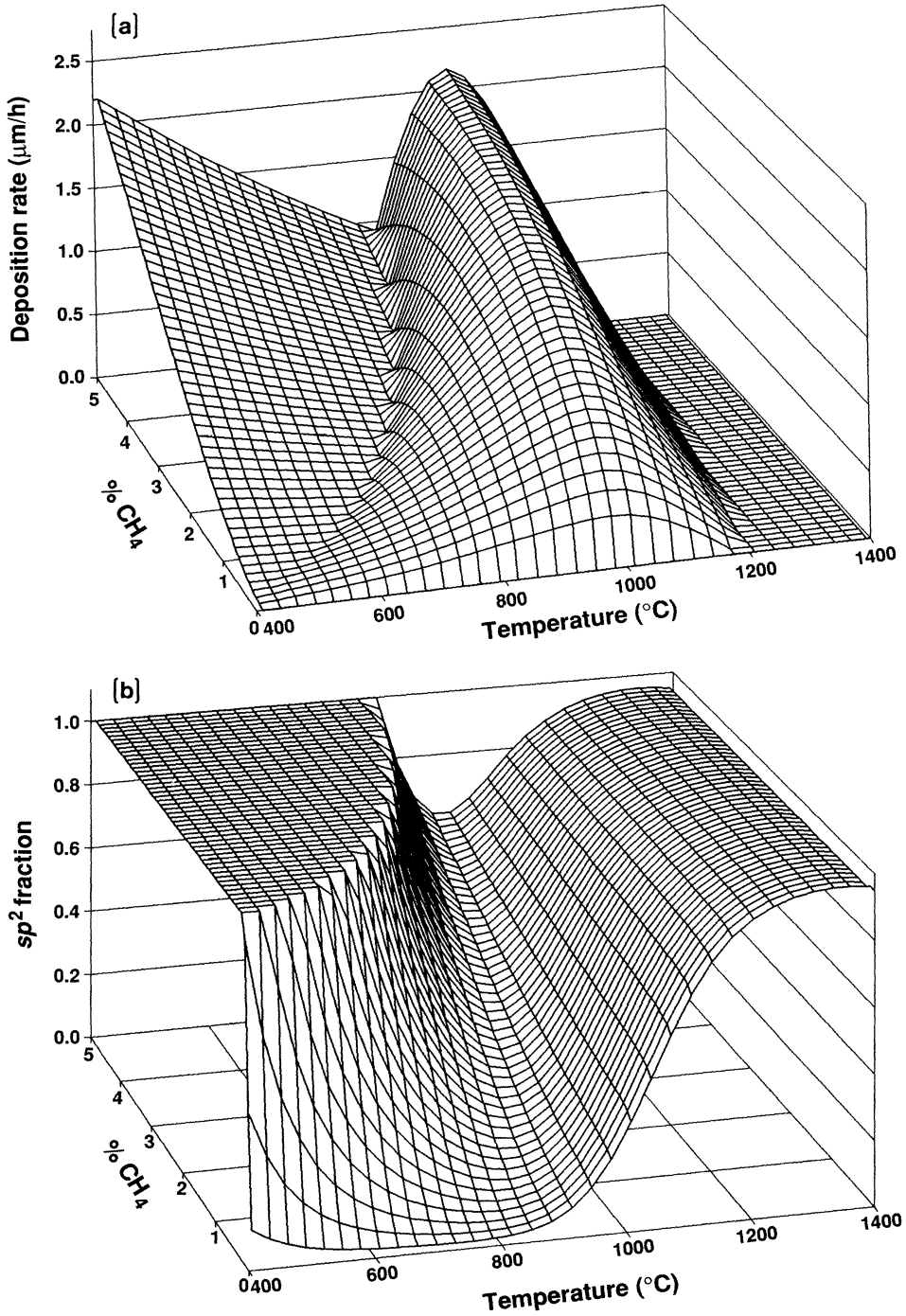

FIG. 4. (a) Deposition rate and (b) film quality vs substrate temperature and initial methane concentration computed at a pressure of 20 Torr.

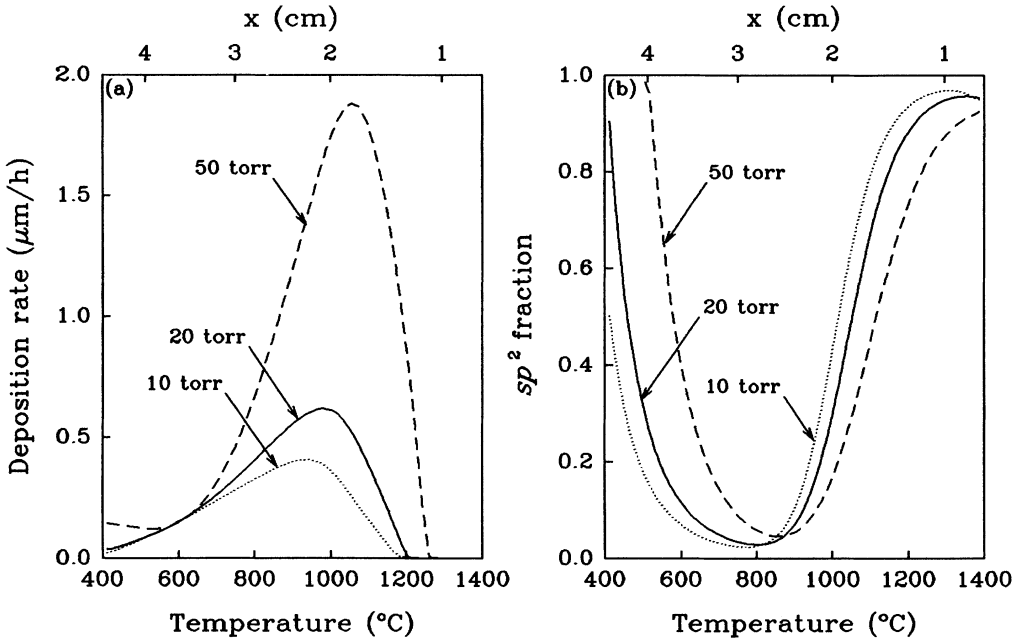

FIG. 5. The effect of total pressure on (a) deposition rate and (b) film quality computed with a (0.3 vol % CH_4)-H_2 mixture.

creases. Such behavior has indeed been observed recently.[110,111,115] The model also reproduces correctly the effect of total pressure:[106,108] with the increase in pressure the deposition rates shift to higher temperatures with the increase in the peak value, as shown in Fig. 5.

C. Deposition reaction pathways

Figure 6 depicts the rates of reactions depositing or removing carbon atoms onto or from the growing surface. The solid line in this figure represents the net deposition rate of the sp^3 carbon phase, i.e., the sum of the net rates of reactions ($s5$), ($s21$), ($s26$), and ($s29$). The individual rates of these reactions are shown in Fig. 7. As can be seen in this figure, by far the fastest reaction channel depositing diamond is reaction ($s5$), the rate of which is identified in Fig. 7 by curve *a*. In other words, the dominant deposition of diamond under the conditions tested occurs via the H-abstraction–C_2H_2-addition reaction mechanism:[26,95] gaseous H atoms abstract H atoms from the diamond surface creating sp^3 surface radical sites,

$$\rightarrow C_d-H+H \rightleftarrows \rightarrow C_d\cdot + H_2$$

[reaction ($s1$)] and the addition of C_2H_2 molecules to these radical sites,

$$\rightarrow C_d\cdot + C_2H_2 \rightarrow \rightarrow C_d-H+H$$

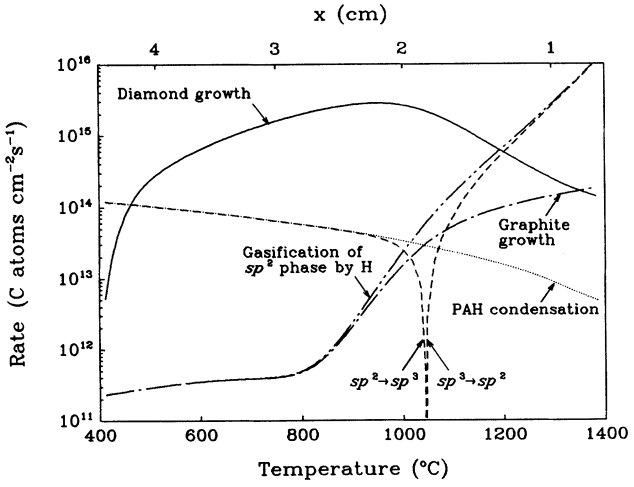

FIG. 6. Comparison of the rates of carbon depositing and removing reactions for the base case, a (0.3 vol % CH_4)-H_2 mixture at a pressure of 20 Torr.

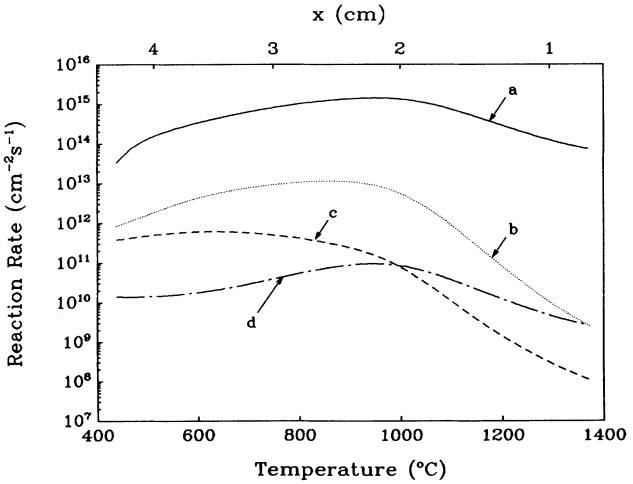

FIG. 7. Comparison of reaction rates of diamond deposition for the base case, a (0.3 vol % CH_4)-H_2 mixture at a pressure of 20 Torr: *a*, reaction ($s5$); *b*, reaction ($s29$); *c*, reaction ($s21$); and *d*, reaction ($s26$).

[reaction ($s5$)] propagates diamond growth. The acetylene addition, reaction ($s5$), is assumed to proceed without activation energy, based on the potential-energy calculations of Huang *et al.*[26]

Other diamond deposition reactions considered in this study are computed to have rates two to four orders of magnitude lower than the rate of the acetylene-addition channel discussed above (Fig. 7). Curve *c* in Fig. 7 identifies the rate of reaction ($s21$), which expresses the formation of sp^3 carbon from surface radical C_d—CH_2—CH_2·. The latter is produced primarily via the addition of gaseous vinyl radicals to C_d surface radicals, reaction ($s23$), followed by reaction ($s24$)–the addition of hydrogen atoms to C_d—$CH=CH_2$ complexes formed in ($s23$). The consecutive addition of CH_3 radicals to surface sites, reactions ($s6$) and ($s12$), accompanied by respective hydrogen abstraction reactions, reactions ($s8$) and ($s16$), is computed to be as fast as the ($s23$)–($s24$) route. This reaction pathway, comprised of alternating CH_3 additions and H abstractions, should be one of the fastest ways of depositing diamond on (111) surface by a CH_3-based mechanism at the conditions when ions are not present at large concentrations. As revealed by the computational results, the reason that this methyl-addition route is much slower than the acetylene-addition route lies in the low concentration of surface complexes C_d—CH_3. This occurs because the formation of C_d—CH_3 in reaction ($s6$) is counteracted by its destruction in reaction ($s7$). When we remove reaction ($s7$) along with similar reactions ($s14$) and ($s15$), whose prototype gas-phase reaction has been questioned,[116] the rate of diamond growth by the methyl-addition reaction channels is increased by a factor of 5 at most. In this case, the rate is limited by the decomposition of the C_d—CH_3 complexes via the reverse of reaction ($s6$). Another limiting factor is the decomposition of C_d—C_2H_5 via reaction ($s16$) followed by the reverse of ($s20$).

Surface complexes C_d—$CH=CH_2$ formed in reaction ($s23$) lead to sp^3 growth not only via their conversion to C_d—CH_2—CH_2· by hydrogen atom addition as discussed above, but also via the formation of a C_d—$CH=CH$· intermediate[26] by H-atom abstraction in reaction ($s26$). The computed rate of the latter reaction is depicted in Fig. 7 by curve *d*. Curve *b* in this figure represents the rate of diamond growth as a result of a combined (sequential) addition of methyl radicals and acetylene molecules—reactions ($s6$), ($s7$), and ($s29$). Such a reaction pathway was suggested by us previously as a possible mechanism for nucleation of the initial kernel that can propagate the epitaxial growth of a diamond layer via the acetylene-addition mechanism.[95] As follows from Fig. 7, the ($s6$)-($s7$)-($s29$) reaction sequence is computed to be the fastest among the methyl-based reaction channels, although still much slower than the acetylene-addition step ($s5$). The latter may explain the existence[5] of an induction period for diamond growth.

In considering the diamond growth reactions discussed above, we assumed that the growth proceeds via a sequence of several steps, e.g.,

$$\rightarrow C_d\cdot + C_2H_4 \rightleftarrows \rightarrow C_d\text{—}CH_2\text{—}CH_2\cdot ,$$

$$\rightarrow C_d\text{—}CH_2\text{—}CH_2\cdot \rightarrow \rightarrow C_d\text{—}H + H$$

[reactions ($s20$) and ($s21$), respectively], instead of more direct chemically activated processes, e.g.,

$$\rightarrow C_d\cdot + C_2H_4 \rightarrow \rightarrow C_d\text{—}H + H$$

[reaction ($s20'$)]. The latter approach is more accurate, but neither the required data nor reliable theory exist to apply it to the problem addressed here. It is reasonable to assume, however, that the reactions of the surface-gas complexes should behave close to the corresponding high-pressure limits, thereby justifying the approach undertaken in this study. Nonetheless, since this assumption affects the important competition[114] between the methyl- and acetylene-addition reaction channels for diamond growth, we performed several numerical sensitivity tests. The inclusion of reaction ($s20'$) with the rate coefficient equal to that of reaction ($s5$) results in about two orders of magnitude larger diamond growth rate via the CH_3-deposition channel ($s21$), yet still about two orders of magnitude slower than the growth via the acetylene-deposition channel ($s5$). It should be pointed out, however, that the assumption $k_{s20'}=k_{s5}$ is quite unrealistic, since we estimate that reaction ($s20'$) should have a significant activation energy, at least 60 kJ/mol, and therefore the discussed test provides an upper-limit estimate for the rate of reaction ($s20'$). Similarly, the inclusion of reaction

$$\rightarrow C_dC_2H_3 + H \rightarrow \rightarrow C_d\text{—}H + H ,$$

proceeding via energized $\rightarrow C_d$—CH_2—CH_2· intermediate complex with an upper-limit rate coefficient, instead of reaction sequence ($s24$)–($s21$) proceeding via thermally stabilized surface species, increases the corresponding flux by one to two orders of magnitude, which is insufficient to effectively compete with reaction ($s5$).

It should be noted that both acetylene- and methyl-addition routes considered in the present study are the same from the point of view that both proceed via the formation of C_d—C_2H_x complexes. These acetylenic surface complexes are so effective because of the high propensity of the triple-bonded carbon to radical addition. One can view the role of acetylene as the "energy storage": the triple bond is formed in the energetic gas-phase environment and the chemical energy of this stable bond is then delivered to the substrate and used in energy-limited surface reactions while still preserving the original C—C bonding. Also, the reversible reactions of the surface complexes can account for the observed experimentally[117] catalytic conversion of C_2H_x to CH_y and vice versa on diamond surfaces.

The curve in Fig. 6 marked "Graphite growth" depicts the growth rate of the sp^2 carbon phase via the H-abstraction–C_2H_2-addition reaction pathways.[94,95,98] This rate is defined in the present work as the sum of the forward rates of reactions ($s36$) and ($s44$). The sum of the reverse rates of these two reactions is shown in Fig. 6 by the curve marked "Gasification of sp^2 phase by H." An inspection of these two curves indicates that both processes are extremely slow, as compared to the dia-

mond growth, at the low- and intermediate-temperature ranges. At higher temperatures, the sp^2 gasification becomes the predominant process while the graphite growth remains relatively slow. A closer examination of the computational results revealed that the major contributor to the graphite growth is reaction ($s44$) and to the sp^2 gasification it is the reverse of reaction ($s36$). In other words, reaction ($s36$), along with reaction ($s39$), runs in reverse. Reaction ($s44$) reverses its direction at temperatures above about 700 °C. Also, reaction ($s35$) reverses its direction at temperatures above 900 °C and reaction ($s40$) and ($s42$) above 1100 °C, and reaction ($s37$) equilibrates at $T > 1200$ °C.

It is somewhat surprising that the growth of the graphitic phase is computed to be so much slower than the growth of diamond. However, this computational prediction can be corroborated by the recent conclusions of Zhu *et al.*[112] and Schroder *et al.*,[118] based on the characterization of diamond films by Raman spectroscopy that graphite inclusions in these films are small, on the order of 1 to 10 nm. The significance of the computational prediction that gasification of the sp^2 carbon phase by hydrogen atoms is not a critical factor at temperatures of diamond deposition will be discussed in Sec. III F.

A most revealing result of the present kinetic study, found to be in accord with experimental observations,[119] is the importance of the $sp^2 \rightleftarrows sp^3$ transformations, represented in our model by reaction ($s45$). At high temperatures, this reaction runs in reverse (see Fig. 6) and signifies graphitization of diamond. At low temperatures, reaction ($s45$) primarily follows condensation of benzene, reaction ($s30$). The latter process, whose rate is represented in Fig. 6 by the curve marked "PAH condensation," was suggested to play a significant role in chemical vapor deposition of diamond in a previous study.[18]

Figure 8 depicts the results of several sensitivity tests demonstrating the significance of the benzene condensation and the $sp^2 \rightleftarrows sp^3$ transformation processes. It should be noticed that the removal of these processes from the model distorts dramatically the predictions: without benzene condensation the model does not predict the low-temperature film characteristics—it predicts 100% diamond phase for temperatures below 700 °C [cf. curves *A* and *B* in Fig. 8(b)]; and without the $sp^2 \rightleftarrows sp^3$ transformation the bell shape of the diamond growth rate dependence on temperature is not reproduced at all [cf. curves *A* and *C* in Fig. 8(a)]. It is clear, therefore, that the rate parameters assigned to these processes significantly influence the numerical predictions of the model. For instance, a comparison of curves *A*, *D*, *E*, and *F* in Fig. 8(b) demonstrates the sensitivity to the sticking probability of benzene condensation: reducing γ from 0.1 to 0.0001, while having no significant effect on the deposition rate and the high-temperature film quality [see Fig. 8(a); only cases *A* and *E* are shown for clarity], decreases substantially (but not entirely) the depositing sp^2 surface coverage at low substrate temperatures. Unfortunately, there are no quantitative data available on the surface sp^2/sp^3 ratio. However, the results computed with different values of γ indicate that a substantially lower sticking probability than 0.1 is also consistent with the qualitative phenomena seen in experiment. Sensitivity analysis for the $sp^2 \rightleftarrows sp^3$ transformation indicated that its rate and thermodynamic parameters affect the temperature of the computed peak deposition rate.

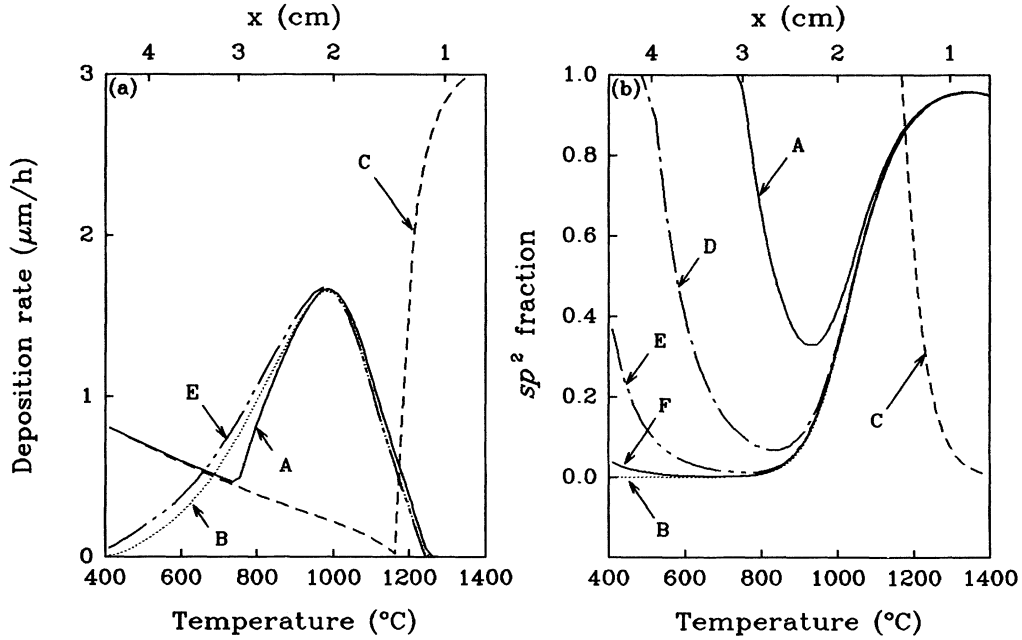

FIG. 8. Sensitivity tests for the (a) deposition rate and (b) film quality computed for a (2.3 vol % CH_4)-H_2 mixture at a pressure of 20 Torr: *A*, mechanism of Table III; *B*, without condensation of benzene, reaction ($s30$); *C*, without $sp^2 \rightleftarrows sp^3$ transformation, reaction ($s45$); *D*, with the sticking probability of benzene condensation $\gamma_{benzene} = 0.01$; *E*, with $\gamma_{benzene} = 0.001$; and *F*, with $\gamma_{benzene} = 0.0001$.

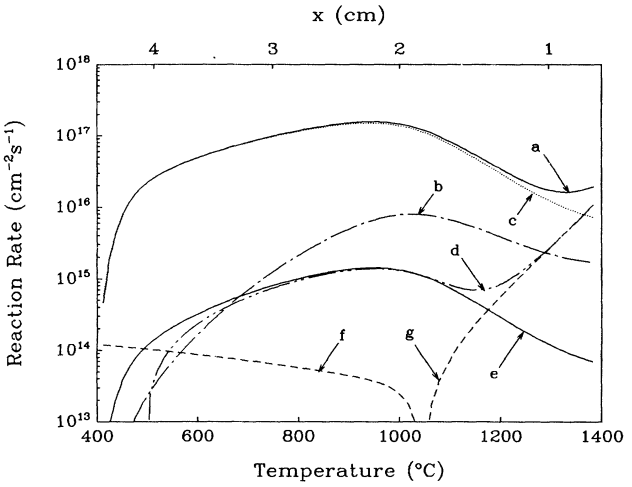

FIG. 9. Rates of selected surface reactions computed for the base case, a (0.3 vol% CH_4)-H_2 mixture at a pressure of 20 Torr: *a*, forward reaction ($s1$); *b*, reverse of reaction ($s1$); *c*, forward reaction ($s4$); *d*, $R_{s1}-R_{s-1}-R_{s4}$; *e*, reaction ($s5$); *f*, forward reaction ($s45$); and *g*, reverse of reaction ($s45$).

D. Temperature dependence

At high temperatures, which in our model correspond to short distances of the substrate surface from the filament, the vapor-deposited diamond sites are rapidly graphitized via reaction ($s45$) and the sp^2 carbon formed is gasified with an equally fast rate by reactions with H atoms, as is evident from the computational results depicted in Fig. 6. In this regime, therefore, the net deposition rate is low and decreases with the increase in temperature [Fig. 4(a)] and the deposited film is predominantly graphite [Fig. 4(b)]. At low temperatures, corresponding to long distances of the substrate surface from the filament, the deposition rate is limited by the rate of production of C_d sites. The number density of these surface radicals is determined by the difference between the rates of reaction ($s1$) producing C_d sites and reaction ($s4$) destroying them (Fig. 9), i.e.,

$$\chi_{C_d}=\frac{k_{s1}}{k_{s4}}\chi_{C_dH}\cdot \tag{19}$$

Because reaction ($s1$) has a substantial activation energy[26] and the rate coefficient of reaction ($s4$) is temperature independent (see Table III), the k_{s1}/k_{s4} ratio is increased with temperature. The number density of available C_dH surface sites is also increased with the increase in temperature in the low-temperature regime, as indicated by the improvement in film quality [Fig. 4(b)]; this occurs due to the reduction in the gas-phase concentration of benzene (Fig. 2) and hence in the rate of its condensation on the growing surface. Thus both factors in Eq. (19) lead to the increase in the C_d number density and therefore in diamond growth rate with temperature. With further increase in temperature, the number density of C_d sites begins to decline due to the reduction in thermodynamic stability of these surface radicals, which expresses itself in the increased rate of reaction

$$C_d \rightarrow C_gH+H$$

[the reverse of reaction ($s45$)]. This explains the bell-shaped temperature dependence of the deposition rate.

The films deposited at low temperatures are computed to contain high sp^2 fractions [Fig. 4(b)]. In this temperature regime, the sp^2-bonded carbon comes primarily from the condensation of benzene. A part of this sp^2 carbon is converted to an sp^3 phase by the addition by hydrogen atoms, reaction ($s45$), as discussed earlier. Considering the possible outcomes of the H addition to an aromatic hydrocarbon adsorbed on a hydrogenated diamond surface, we conclude that the sp^3 carbon phase formed in the low-temperature regime must contain an amorphous, diamondlike component rather than purely diamond crystallites. This may explain the increased imperfection in diamond film morphology observed in experimental studies at low substrate temperatures.[109,120]

The difference in the nature of the sp^2 carbon phases formed in different temperature regimes can be further demonstrated by the results computed for situations when the substrate and the gas-phase temperatures are different from one another (Fig. 10). Such a geometry can be imposed on our model by considering a constant-temperature substrate placed along the reactor wall. In these computations, the reaction rates of gas-surface reactions were multiplied by the term $(T_g/T_s)^{1/2}$. In doing so, we assumed, at the present level of modeling, that the frequency of collisions of a gaseous species with a surface site is determined by the gas-phase temperature T_g, but the probability of reaction (i.e., the transition state) is determined by the surface temperature T_s.

The results depicted in Fig. 10(b) clearly indicate that the computed film quality at the high substrate temperatures is independent of the gas-phase temperature—it is determined by the graphitization process, the reverse of reaction ($s45$). At the low substrate temperatures, the film quality is dramatically worsened with the decrease in the gas-phase temperature, i.e., with moving away from the filament, as a result of the increased concentration of benzene and, therefore, the increased rate of benzne condensation on the substrate surface via reaction ($s30$). In contrast to the computed film quality, the bell shape of the deposition rate dependence on the substrate temperature is computed to be independent of the gas-phase temperature [Fig. 4(a)]. Our model predicts that larger deposition rates and a better film quality are obtained when the gas-phase temperature in the deposition zone is higher than the substrate temperature.

E. Effects of initial methane concentration and pressure

The gas-phase kinetic model predicts that an increase in the initial methane concentration decreases the concentration of hydrogen atoms and increases the concentrations of hydrocarbon products including acetylene and benzene, as demonstrated in Fig. 11. These computed trends are in general agreement with experimental observations.[15,20] A detailed analysis of the computational results revealed that at low methane concentrations, the decrease in the H concentration leads to an increase in the

number density of C_d surface sites as a result of the competition between the H-abstraction forming C_d, reaction ($s1$), and the H-addition removing these radical sites, reaction ($s4$). Accompanied with the rise in acetylene concentration, this increases the rate of reaction ($s5$) in the low methane concentration regime, as shown in Fig. 12.

With the increase in the methane concentration, the number density of C_dH sites decreases because they are being covered by the increasing surface condensation of benzene. This phenomenon counteracts the promoting factors discussed above and eventually leads to a decline in the rate of reaction ($s5$). Ultimately, the condensation

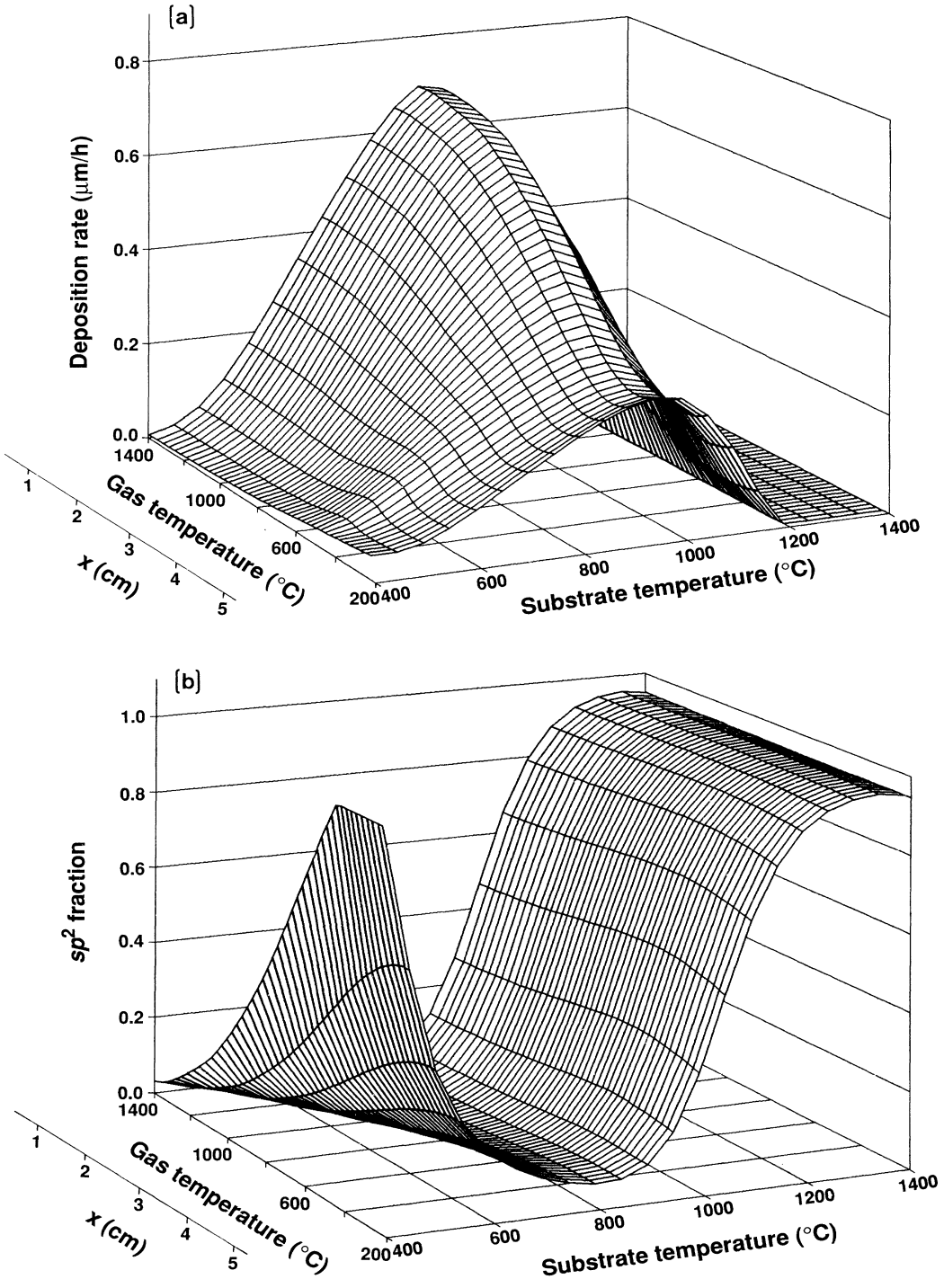

FIG. 10. (a) Deposition rate and (b) film quality vs substrate and gas-phase temperatures computed for the base case, a (0.3 vol % CH_4)-H_2 mixture at a pressure of 20 Torr.

of benzene becomes the dominant carbon deposition process, as can be seen in Fig. 12. The increased role of benzene condensation becomes also apparent when comparing the major carbon deposition fluxes of the base case (Fig. 6) with those computed at a higher methane concentration depicted in Fig. 13.

Thus, at higher methane concentrations, the net film deposition rate is determined primarily by the balance of diamond growth in reaction ($s5$) and the condensation of benzene onto the growing surface. The film quality is predicted by the model to deteriorate with the increase in the initial concentration of methane. At low CH_4 concentrations, when reaction ($s5$) dominates, the deposited film consists of diamond. At higher methane concentrations, when benzene condensation catches up with diamond deposition, the film should contain amorphous carbon, formed by the H addition to condensing benzene in reaction ($s45$). At even higher methane concentrations,

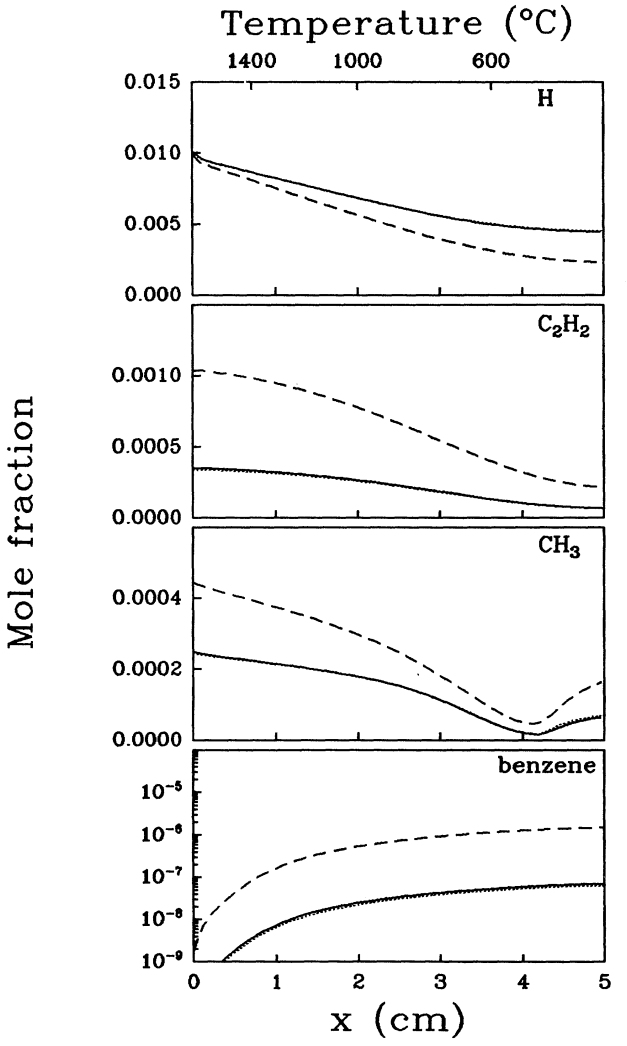

FIG. 11. Comparison of several gaseous species concentrations computed at a pressure of 20 Torr: solid lines, base case, (0.3 vol % CH_4)-H_2; dashed lines, (2.3 vol % CH_4)-H_2; and dotted lines, (2.3 vol % CH_4)-(1.0 vol % O_2)-H_2 (dotted and solid lines practically overlap each other).

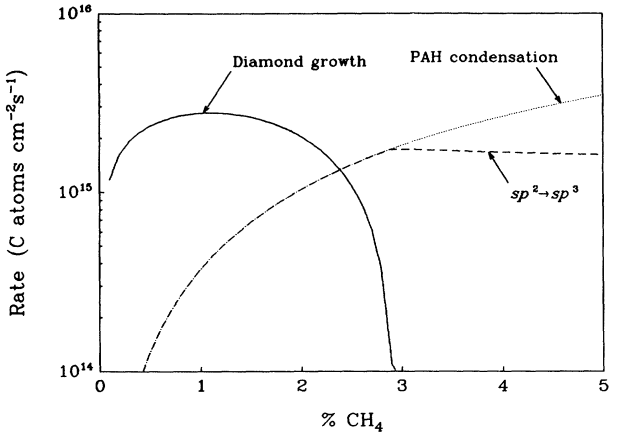

FIG. 12. Main deposition rates computed at a temperature of 800 °C and a pressure of 20 Torr: solid line, diamond growth via reaction ($s5$); dotted line, condensation of benzene, reaction ($s30$); and dashed line, conversion of sp^2 to sp^3, reaction ($s45$).

as the $sp^2 \rightarrow sp^3$ transformation by the H addition can no longer follow the benzene condensation, the depositing film should consist of predominantly graphite.

Analysis of the computational results indicated that the effect of pressure is essentially explained by the effect of the initial methane concentration. One may notice, however, that the computed shift of the temperature of the maximum deposition rate is more pronounced for the pressure effect (cf. Figs. 4 and 5). As discussed earlier, the decline in the deposition rate with the increase in temperature is explained by the decreasing stability of C_d surface radicals. Assuming that at these conditions the $C_gH + H \rightleftarrows C_d$ transformation is in the state of partial equilibrium, and the computational results support this assumption at not so high temperatures, we obtain

$$\frac{\chi_{C_dH}}{\chi_{C_gH}} = \frac{k_{s1}[H]}{k_{s4}K_{s45}}, \tag{20}$$

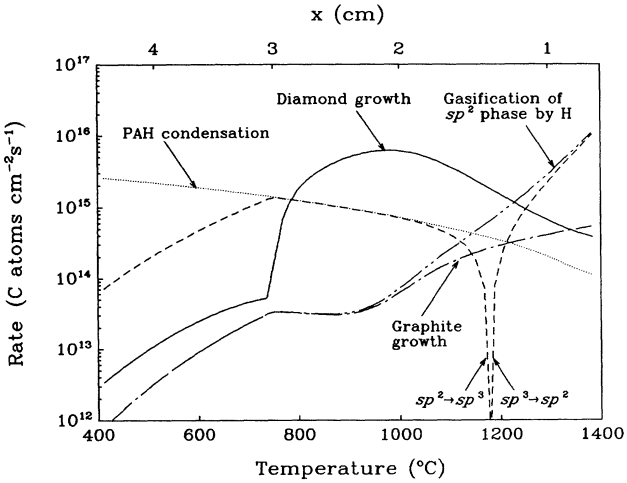

FIG. 13. Comparison of the rates of carbon depositing and removing reactions computed for a (2.3 vol % CH_4)-H_2 mixture and a pressure of 20 Torr.

where K_{s45} is the equilibrium constant of reaction ($s45$) and Eq. (19) was used for the number density of the C_d radical sites. Equation (20) implies that the surface fraction of the C_dH sites at a given temperature, and hence the position of the peak in the deposition rate, is determined by the concentration of hydrogen atoms. It turns out that for the conditions tested the increase in pressure results in a larger reduction in the H concentration than the increase in the initial methane concentration.

F. Role of hydrogen

The role of hydrogen in vapor-activated deposition of diamond has been the focus of attention because it is only after a large excess of hydrogen was used in the process that μm/h growth rates were obtained.[2,3,12,121] Several possible explanations have been proposed (see recent articles for review,[2,3,5] and analyses[13,18,122]). Most of the proposals implicate atomic hydrogen, most notably the preferential etching of graphite over diamond, advanced by the Russian scientists[12] and now adopted widely, and stabilization of the diamond surface. Using the developed model, we now examine the factors affected by the presence of hydrogen.

Figure 9 presents the largest computed rates of reactions involving hydrogen atoms. An inspection of this figure indicates that the fastest reactions among them are the H abstraction, reaction ($s1$), which activates the diamond surface by producing radicals sites, and the recombination of H atoms with these radical sites, reaction ($s4$). In other words, these two reactions principally control the number density of active C_d sites. One may notice that the rate difference of these two reactions (curve d in Fig. 9) practically overlays with the diamond growth flux at the low and medium temperatures and with the rate of graphitization at the high temperatures. The next important processes are the transformation of sp^2 to sp^3 at low temperatures and the gasification of the sp^2 phase (etching) at high temperature, both processes governed by the addition of hydrogen atoms to unsaturated carbon bonds. As mentioned earlier, the sp^2 gasification by H atoms is computed to be a slow process at temperatures of diamond deposition. That is, our model does not support the theory of preferential etching advanced[9-12] to explain the kinetic competition between diamond and nondiamond phases.

The present computational results fully support the prediction made by us previously[18] that the main effect the addition of hydrogen has on diamond deposition is the suppression of the formation of aromatic species in the gas phase by H_2. A computer simulation at the same conditions as the base case but with hydrogen replaced by argon in the initial mixture resulted in a purely sp^2 film whose deposition rate decreases with temperature monotonically.

G. Role of oxygen

Perhaps the most intriguing technological advancements made since the addition of hydrogen is the improved characteristics of diamond deposition with the addition of oxygen[4,5,20,115,123,124] and the growth of diamond films in hydrocarbon flames,[123,125,126] pioneered by Hirose and co-workers. It was of interest, therefore, to investigate what possible effects on diamond growth can be predicted by our model when oxygen is introduced into the system. Since no detailed experimental information (e.g., temperature profiles) on oxidative environments depositing diamond films is available, we performed computational tests using the reactor geometry adopted in the present study for the oxygen-free analysis and assuming that the initial mixture contains a small amount of oxygen, such that the temperature profile should not be significantly different from the assumed profile.

The results of such simulations indicated that the addition of small amounts of oxygen does not necessarily increase the deposition rate but substantially improves the film quality, especially at low temperatures (Fig. 14). This computational prediction[127] is now supported by experimental observations.[124] The model predicts the decrease in the concentrations of hydrocarbon species (Fig. 11), also in accord with experimental findings.[115,128]

An analysis of the computational results indicated that the improvement in film quality with the addition of oxygen results from the decrease in the concentration of benzene, as was hypothesized by us previously.[18] The latter is caused by the oxidation of hydrocarbon precursors to benzene. In reactor geometries like the one considered in this study—after being exposed to a very high temperature, the reactive gas flows along a decreasing temperature profile—the formation of aromatic species from a hydrocarbon mixture occurs when the gas cools to temperatures around 1000 °C.[18,129,130] Under such conditions, the addition of small amounts of oxygen to the inlet stream results in practically stoichiometric oxidation of carbon prior to the gas reaching the aromatics-forming region.[129] In fuel-rich mixtures, because of the relatively low concentration of OH and hence a slow rate of CO conversion to CO_2, the oxidized carbon is accumulated in the form of CO. Based on these considerations, we chose to compare the results obtained in the computer simulation of a (2.3 vol % CH_4)-(1.0 vol % O_2)-H_2 mixture with those of a (0.3 vol % CH_4)-H_2 mixture, because in both cases the total amount of carbon accumulated in hydrocarbon species after the hot-filament zone should be the same.

Comparing these results, we note that the species concentrations (Fig. 11) and the deposition characteristics (Fig. 14) are indeed very close to one another in the two cases. In these computations, as typical for the present study, the substrate temperature was assumed to be equal to the gas temperature. When the gas and the substrate temperatures are allowed to vary separately from one another, the film quality computed for a (2.3 vol % CH_4)-(1.0 vol % O_2)-H_2 mixture (Fig. 15) is notably improved over that for a (0.3 vol % CH_4)-H_2 mixture [Fig. 10(b)] at low substrate temperatures. This difference is caused by the gasification of the sp^2 carbon by OH radicals, reaction ($s49$). The rate of this reaction is denoted by a solid curve marked "Gasification of sp^2 phase by OH" in Fig. 16; this figure depicts the rates of major car-

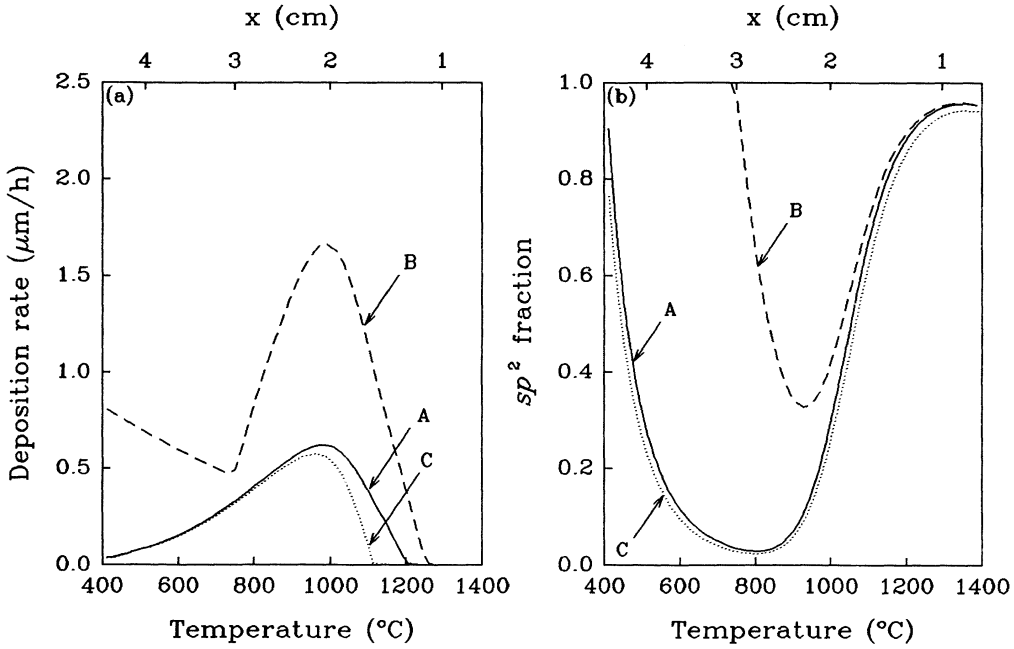

FIG. 14. The effect of oxygen addition on the (a) deposition rate and (b) film quality computed at a pressure of 20 Torr: *A*, base case, (0.3 vol % CH_4)-H_2; *B*, (2.3 vol % CH_4)-H_2; and *C*, (2.3 vol % CH_4)-(1.0 vol % O_2)-H_2.

bon depositing and removing reactions computed for the oxygen-containing mixture.

IV. SUMMARY AND CONCLUSIONS

A chemical kinetic model is developed that includes detailed descriptions of both gas-phase and surface processes occurring in gas-activated deposition of diamond films on diamond (111) surface. The model was tested by simulating diamond film deposition in a hot-filament reactor using methane-hydrogen, methane-argon, and methane-oxygen-hydrogen gas mixtures. The gas-phase part of the model includes transport phenomena and pre-

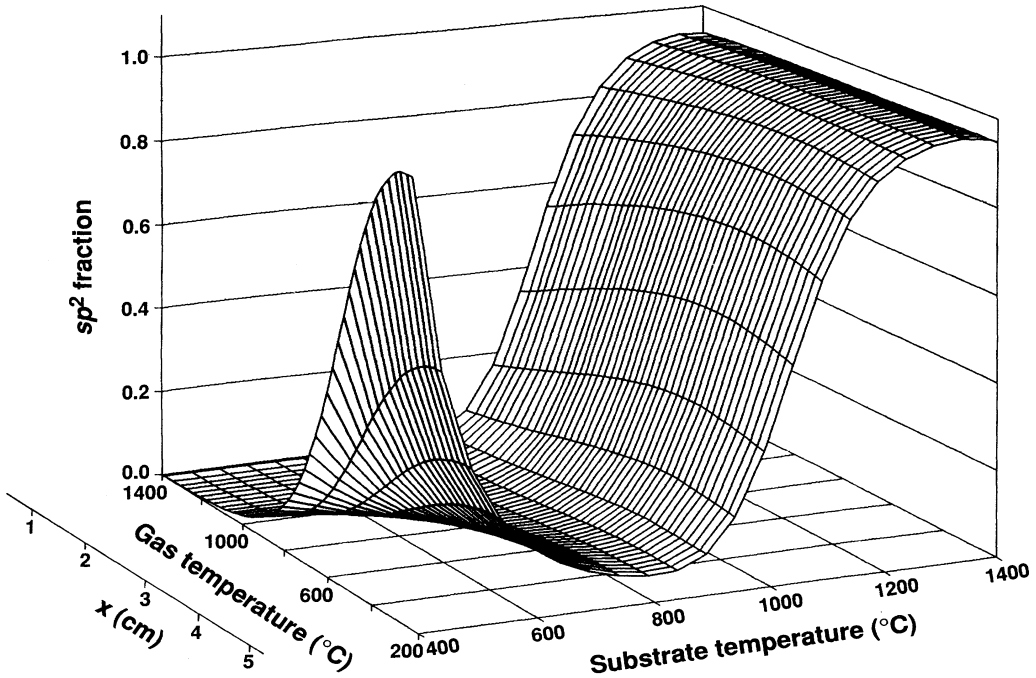

FIG. 15. Film quality vs substrate and gas-phase temperatures computed for a (2.3 vol % CH_3)-(1.0 vol % O_2)-H_2 mixture and a pressure of 20 Torr.

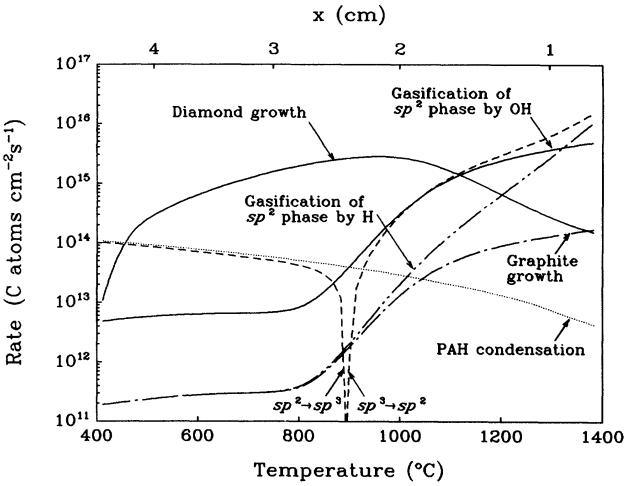

FIG. 16. Comparison of the rates of carbon depositing and removing reactions for a (2.3 vol% CH_4)-(1.0 vol% O_2)-H_2 mixture and a pressure of 20 Torr.

dicts correctly the measured concentrations of major gaseous species. The surface part of the model reproduces the general experimental trends—the effects of temperature, pressure, initial methane concentration, and the addition of oxygen—for the growth rate and film quality.

The analysis of the computational results along with various sensitivity tests led us to the following conclusions.

(i) The quantitative prediction of the gas-phase environment in the film deposition zone depends critically on the precise knowledge of the gas history not only in the post-filament zone but also in pre- and near-filament zones.

(ii) Under the conditions studied, diamond grows predominantly by the addition of acetylene to sp^3-hybridized surface radicals C_d. The contribution to the growth by other species—methyl, ethyl, ethylene, and vinyl—is computed to be extremely slow under the tested conditions. The reaction-path analysis indicates that diamond deposition by these species proceeds via the formation of acetylenic or ethylenic intermediate complexes on the growing surface.

(iii) The reaction "bottleneck" of diamond deposition at low substrate temperatures is the formation of C_d radicals. Their formation rate is determined by the balance between the H-abstraction $C_dH+H \rightarrow C_d+H_2$ and recombination $C_d+H \rightarrow C_dH$ reactions. This rate increases with temperature because the former reaction has a substantial activation energy whereas the latter does not. At higher substrate temperatures, the thermodynamic stability of C_d radicals becomes the limiting factor: the sp^3-hybridized C_d sites decompose forming an sp^2 graphitic phase.

(iv) The chemical growth of the sp^2 graphite phase is computed to be much slower than the growth of diamond.

(v) At low substrate temperatures, condensation of benzene from the gas phase onto the growing surface competes with the diamond growth process by covering the available sp^3 diamond sites. The condensing aromatic molecules are converted into an amorphous sp^2/sp^3 carbonaceous network by the addition reactions of hydrogen atoms.

(vi) The main factors affecting the deposition characteristics with the increase in the initial concentration of methane are the increase in the aromatics formation and, to a lesser degree, the decrease in the H-atom concentration. The former factor reduces the quality of the film, whereas the latter causes the shift of the peak deposition rate to higher substrate temperatures. The effect of pressure is essentially the concentration effect.

(vii) The key role of hydrogen and oxygen in diamond deposition is to suppress the formation of aromatic species in the gas phase and thereby to prevent their condensation onto the growing surface.

(viii) The major reactions of hydrogen atoms in the surface processes are the H-atom abstraction, which activates the surface by creating radical sites; recombination with these surface radicals; and the addition to unsaturated carbon—carbon bonds, thereby converting aromatics into amorphous carbon at low temperatures and gasifying graphite at high temperatures.

(ix) Gasification of sp^2 carbon by OH radicals, which is computed to be much faster than that by H atoms when oxygen is added to the mixture, contributes to the improved quality of diamond films deposited at lower substrate temperatures.

Taken together, these conclusions imply that our model does not support the theory of preferential etching advanced to explain the kinetic competition between diamond and nondiamond phases. Instead, it establishes the critical role of aromatics condensation and interconversion of sp^2 and sp^3 carbon phases mediated by hydrogen atoms in gas-activated deposition of diamond films.

ACKNOWLEDGMENTS

The computations were performed using the facilities of the Pennsylvania State University Center for Academic Computing. The work was supported in part by Innovative Science and Technology Program of the Strategic Defense Initiative Organization (SDIO/IST) via the U.S. Office of Naval Research, under Contract No. N00014-86-K-0443.

[1]R. C. DeVries, Annu. Rev. Mater. Sci. **150**, 161 (1987).
[2]J. H. Angus and C. C. Hayman, Science **241**, 913 (1988).
[3]J. C. Angus, in *Diamond and Diamond-Like Films,* edited by J. P. Dismukes (The Electrochemical Society, Pennington, NJ, 1989), p. 1.
[4]S. Matsumoto, Ref. 3, p. 50.
[5]K. E. Spear, J. Am. Ceram. Soc. **72**, 171 (1989).
[6]P. K. Bachmann and R. Messier, Chem. Eng. News **67**, 24

(1989).
[7]M. N. Yoder, in *Novel Refractory Semiconductors,* edited by D. Emin, T. L. Aselage, and C. Wood (Materials Research Society, Pittsburgh, 1987), p. 315.
[8]A. Hara and N. Fujimori, Ref. 3, p. 14.
[9]B. V. Derjaguin and D. V. Fedoseev, Sci. Am. **233**, 102 (1975).
[10]B. V. Deryagin and D. V. Fedoseev, *Growth of Diamond and Graphite from the Gas Phase* (Nauka, Moscow, 1977), in Russian [English translation in *Surf. Coatings Technol.* **38**, 131 (1989)].
[11]D. V. Fedoseev, V. P. Varnin, and B. V. Deryagin, Russ. Chem. Rev. **53**, 435 (1984).
[12]D. V. Fedoseev, B. V. Deryagin, I. G. Varshavskaya, and A. S. Semenova-Tyan-Shanskaya, Ref. 10, p. 1.
[13]E. S. Machlin, J. Mater. Res. **3**, 958 (1988).
[14]M. Sommer, K. Mui, and F. W. Smith, Solid State Commun. **69**, 775 (1989).
[15]J. E. Butler and F. C. Celii, Ref. 3, p. 317.
[16]W. Piekarczyk, R. Roy, and R. Messier, J. Cryst. Growth **98**, 765 (1989).
[17]L. E. Kline, W. D. Partlow, and W. E. Bies, J. Appl. Phys. **65**, 70 (1989).
[18]M. Frenklach, J. Appl. Phys. **65**, 5142 (1989).
[19]S. J. Harris, J. Appl. Phys. **65**, 3044 (1989).
[20]J. A. Mucha, D. L. Flamm, and D. E. Ibbotson, J. Appl. Phys. **65**, 3448 (1989).
[21]W. C. Roman and M. B. Colket III, Ref. 3, p. 330.
[22]G. Janssen, W. J. P. van Enckevort, and L. J. Giling, Ref. 3, p. 508.
[23]Y. Matsui and M. Sahara, Jpn. J. Appl. Phys. **28**, 1023 (1989).
[24]M. Tsuda, M. Nakajima, and S. Oikawa, J. Am. Chem. Soc. **108**, 5780 (1986).
[25]M. Tsuda, M. Nakajima, and S. Oikawa, Jpn. J. Appl. Phys. Phys. **26**, L527 (1987).
[26]D. Huang, M. Frenklach, and M. Maroncelli, J. Phys. Chem. **92**, 6379 (1988).
[27]S. J. Harris, A. M. Weiner, and T. A. Perry, Appl. Phys. Lett. **53**, 1605 (1988).
[28]R. J. Kee, J. F. Grgar, M. D. Smooke, and J. A. Miller, Sandia Report No. SAND85-8240, Livermore, CA, 1985.
[29]R. J. Kee, J. Warnatz, and J. A. Miller, Sandia Report No. SAND83-8209, Livermore, CA, 1983.
[30]R. C. Reid, J. M. Prausnitz, and T. K. Sherwood, *The Properties of Gases and Liquids* (McGraw-Hill, New York, 1975), p. 678.
[31]A. C. Hindmarsh, in *Scientific Computing—Applications of Mathematics and Computing to the Physical Sciences,* edited by R. S. Stepleman, M. Carver, R. Peskin, W. F. Ames, and R. Vichnevetsky (North-Holland, Amsterdam, 1983), p. 55; A. C. Hindmarsh, ACM-SIGNUM NewsLetter **15**, 10 (1980).
[32]M. Frenklach, H. Wang, and M. J. Rabinowitz (unpublished).
[33]H. Wang and M. Frenklach, in *Chemical and Physical Processes in Combustion, Twenty-Second Fall Technical Meeting of the Eastern States Section of the Combustion Institute* (The Eastern Section of the Combustion Institute, Albany, NY, 1989), p. 12-1.
[34]M. Frenklach, in *Numerical Approaches to Combustion Modeling,* edited by E. S. Oran and J. P. Boris (American Institute of Aeronautics and Astronautics Progress Series, Washington, D.C., in press).
[35]J. Warnatz, in *Combustion Chemistry,* edited by W. C. Gardiner, Jr. (Springer-Verlag, New York, 1984), p. 197.
[36]T. Yuan, C. Wang, C.-L. Yu, M. Frenklach, and M. J. Rabinowitz, J. Phys. Chem. (to be published).
[37]K. Natarajan and P. Roth, Combust. Flame **70**, 267 (1987).
[38]J. V. Michael and J. W. Sutherland, J. Phys. Chem. **92**, 3853 (1988).
[39]G. Dixon-Lewis, in *Complex Chemical Reaction Systems. Mathematical Modelling and Simulation,* edited by J. Warnatz and W. Jäger (Springer-Verlag, Berlin, 1987), p. 265.
[40]P. H. Stewart, T. Rothem, and D. M. Golden, *Twenty-Second Symposium (International) on Combustion* (The Combustion Institute, Pittsburgh, 1989), p. 943.
[41]P. H. Stewart, G. P. Smith, and D. M. Golden, Int. J. Chem. Kinet. **21**, 923 (1989).
[42]D. L. Baulch, M. Bowers, D. G. Malcolm, and R. T. Tuckerman, J. Phys. Chem. Ref. Data **15**, 465 (1986).
[43]J. W. Sutherland, J. V. Michael, and R. B. Klemm, J. Phys. Chem. **90**, 5941 (1986).
[44]K. A. Bhaskaran, P. Frank, and T. Just, *Proceedings of the Twelfth International Symposium of Shock Tube and Waves* (Dekker, Jerusalem, 1980), p. 503.
[45]I. R. Slagle, D. Sarzynski, and D. Gutman, J. Phys. Chem. **91**, 4375 (1987).
[46]T. K. Choudhury and M. C. Lin, Combust. Sci. Technol. **64**, 19 (1989).
[47]S. Zabarnick, J. W. Fleming, and M. C. Lin, Int. J. Chem. Kinet. **20**, 117 (1988).
[48]T. K. Choudhury, W. A. Sanders, and M. C. Lin, J. Phys. Chem. **93**, 5143 (1989).
[49]R. S. Timonen, E. Ratajczak, D. Gutman, and A. F. Wagner, J. Phys. Chem. **91**, 5325 (1987).
[50]C. W. Larson, P. H. Stewart, and D. M. Golden, Int. J. Chem. Kinet. **20**, 27 (1988).
[51]P. H. Stewart, C. W. Larson, and D. M. Golden, Combust. Flame **75**, 25 (1989).
[52]N. Cohen and K. R. Westberg, J. Phys. Chem. Ref. Data **12**, 531 (1983).
[53]P. H. Stewart and D. M. Golden (private communication).
[54]P. Frank and M. Braun-Unkhoff, Ref. 39, p. 69.
[55]M. A. Weissman and S. W. Benson, J. Phys. Chem. **92**, 4080 (1988).
[56]F. P. Tully, Chem. Phys. Lett. **143**, 510 (1988).
[57]A. Liu, W. A. Mulac, and C. D. Jonah, J. Phys. Chem. **92**, 3828 (1988).
[58]P. Heinemann, R. Hofmann-Sievert, and K. Hoyermann, *Twenty-First Symposium (International) on Combustion* (The Combustion Institute, Pittsburgh, 1988), p. 865.
[59]A. E. Lutz, R. J. Kee, J. A. Miller, H. A. Dwyer, and A. K. Oppenheim, Ref. 40, p. 1683.
[60]I. R. Slagle, J.-Y. Park, M. C. Heaven, and D. Gutman, J. Am. Chem. Soc. **106**, 4356 (1984).
[61]V. S. Rao and G. B. Skinner, J. Phys. Chem. **92**, 6313 (1988).
[62]T. Tanzawa and W. C. Gardiner, Jr., J. Phys. Chem. **84**, 236 (1980); Y. Hidaka, C. S. Eubank, W. C. Gardiner, Jr., and S. M. Hwang, *ibid.* **88**, 1006 (1984); S. M. Hwang, W. C. Gardiner, Jr., M. Frenklach, and Y. Hidaka, Combust. Flame **67**, 65 (1987); W. Gardiner, T. Tanzawa, T. Koike, and K. Morinaga, Bull. Chem. Soc. Jpn. **58**, 1851 (1985).
[63]K. Mahmud and A. Fontijn, J. Phys. Chem. **91**, 1918 (1987).
[64]P. Frank, K. A. Bhaskaran, and T. Just, Ref. 58, p. 885.
[65]A. Liu, W. A. Mulac, and C. D. Jonah, J. Phys. Chem. **92**, 5942 (1988).
[66]J. A. Miller and C. F. Melius, Ref. 40, p. 1031.
[67]S. M. Hwang, W. C. Gardiner, Jr., and J. Warnatz, Prog. Aeronaut. Astronaut. **95**, 198 (1984).
[68]W. Tsang and R. F. Hampson, J. Phys. Chem. Ref. Data **15**, 1087 (1985).

[69]J. Warnatz, H. Bockhorn, A. Moser, and H. W. Wenz, *Nineteenth Symposium (International) on Combustion* (The Combustion Institute, Pittsburgh, 1982), p. 197.
[70]T. Böhland, F. Temps, and H. Gg. Wagner, Ref. 58, p. 841.
[71]J. H. Kiefer, M. Z. Al-Alami, and K. A. Budach, J. Phys. Chem. **86**, 808 (1982).
[72]A. Fahr and S. E. Stein, Ref. 40, p. 885.
[73]M. A. Weissman and S. W. Benson, Int. J. Chem. Kinet. **16**, 307 (1984).
[74]J. H. Kiefer, K. I. Mitchell, R. D. Kern, and J. N. Yong, J. Phys. Chem. **92**, 677 (1988).
[75]A. Liu, W. A. Mulac, and C. D. Jonah, J. Phys. Chem. **92**, 131 (1988).
[76]R. P. Duran, V. T. Amorebieta, and A. J. Colussi, J. Phys. Chem. **92**, 636 (1988).
[77]I. R. Slagle, J. R. Bernherdt, and D. Gutman, Ref. 40, p. 953.
[78]P. R. Westmoreland, A. M. Dean, J. B. Howard, and J. P. Longwell, J. Phys. Chem. **93**, 8171 (1989).
[79]M. J. S. Dewar, W. C. Gardiner, Jr., M. Frenklach, and I. Oref, J. Phys. Chem. **109**, 4456 (1987).
[80]J. H. Kiefer, L. J. Mizerka, M. R. Patel, and H. C. Wei, J. Phys. Chem. **89**, 2013 (1985).
[81]S. Madronich and W. Felder, J. Phys. Chem. **89**, 3556 (1985).
[82]V. S. Rao and G. B. Skinner, J. Phys. Chem. **92**, 2442 (1988).
[83]C.-Y. Lin and M. C. Lin, *Chemical and Physical Processes in Combustion, Twentieth Fall Technical Meeting of the Eastern States Section of the Combustion Institute* (The Eastern Section of the Combustion Institute, Gaithersburg, MD, 1987), p. 7-1.
[84]K. Luther and J. Troe, in *Reactions of Small Transient Species: Kinetics and Energetics,* edited by A. Fontijn and M. A. A. Clyne (Academic, London, 1983), p. 63.
[85]W. C. Gardiner, Jr. and J. Troe, Ref. 35, p. 173.
[86]D. M. Golden and C. W. Larson, *Twentieth Symposium (International) on Combustion* (The Combustion Institute, Pittsburgh, 1985), p. 595.
[87]R. G. Gilbert and S. C. Smith, Quantum Chemistry Program Exchange, Program No. 460, Indiana University, Bloomington, IN, 1986.
[88]M. Frenklach, D. W. Clary, T. Yuan, W. C. Gardiner, Jr., and S. E. Stein, Combust. Sci. Technol. **50**, 79 (1986).
[89]M. Frenklach, T. Yuan, and M. K. Ramachandra, Energy & Fuels **2**, 462 (1988).
[90]A. Burcat, Ref. 35, p. 455.
[91]R. J. Kee, F. M. Rupley, and J. A. Miller, Sandia Report No. SAND87-8215, Livermore, CA, 1987.
[92]P. G. Green, J. L. Kinsey, and R. W. Field, J. Chem. Phys. **91**, 5160 (1989).
[93]S. E. Stein and A. Fahr, J. Phys. Chem. **94**, 3714 (1985).
[94]M. M. Frenklach, in *Carbon in the Galaxy: Studies from Earth and Space,* edited by J. Tarter, S. Chang, and D. J. DeFrees (NASA Conference Publication 3061, Moffett, CA, 1990), p. 259.
[95]M. Frenklach and K. E. Spear, J. Mater. Res. **3**, 133 (1988).
[96]D. Bernfeld and G. B. Skinner, J. Phys. Chem. **87**, 3732 (1983).
[97]K. Tabayashi and S. H. Bauer, Combust. Flame **34**, 63 (1979).
[98]M. Frenklach, D. Clary, W. C. Gardiner, Jr., and S. E. Stein, Ref. 86, p. 887.
[99]K. G. Neoh, J. B. Howard, and A. F. Sarofim, *Particulate Carbon: Formation During Combustion* (Plenum, New York, 1981), p. 261.
[100]W. C. Gardiner, Jr., *Rates and Mechanisms of Chemical Reactions* (Benjamin, Menlo Park, CA, 1972), p. 75.
[101]R. B. Bird, W. E. Stewart, and E. N. Lightfoot, *Transport Phenomena* (Wiley, New York, 1960), p. 508.
[102]G. A. Somorjai, J. Phys. Chem. **94**, 1013 (1990).
[103]M. Frenklach and W. C. Gardiner, Jr., J. Phys. Chem. **88**, 6263 (1984).
[104]M. Frenklach, Chem. Eng. Sci. **40**, 1843 (1985).
[105]M. Frenklach, Ref. 39, p. 2.
[106]B. V. Spitsyn and L. L. Bouilov, in *Extended Abstracts. Diamond and Diamond-Like Materials Synthesis,* edited by G. H. Johnson, A. R. Badzian, and M. W. Geis (Materials Research Society, Pittsburgh, 1988), p. 3.
[107]D. V. Fedoseev, K. S. Uspenskaya, V. P. Varnin, and S. P. Vnukov, Bull. Acad. Sci. USSR Div. Chem. Sci. **27**, 1088 (1978).
[108]B. V. Deryagin, L. L. Bouilov, and B. V. Spitsyn, Arch. Nauki Mater. **7**, 111 (1986).
[109]W. Zhu, R. Messier, and A. R. Badzian, Ref. 3, p. 61.
[110]T. McKenna, M.S. thesis, Pennsylvania State University, 1990.
[111]K. M. Tomaswick and J. N. Bruggeman, in *Technology Update on Diamond Films,* edited by R. P. H. Chang, D. Nelson, and A. Hiraki (Materials Research Society, Pittsburgh, 1989), p. 83.
[112]W. Zhu, C. A. Randell, A. R. Badzian, and R. Messier, J. Vac. Sci. Technol. A **7**, 2315 (1989).
[113]F. G. Celii, P. E. Pehrsson, H. T. Wang, and J. E. Butler, Appl. Phys. Lett. **52**, 2045 (1988).
[114]W. A. Yarbrough and R. Messier, Science **247**, 688 (1990).
[115]T. Kawato and K. Kondo, Jpn. J. Appl. Phys. **26**, 1429 (1987).
[116]R. A. Back, Can. J. Chem. **61**, 916 (1983).
[117]C. J. Chu, B. J. Bai, M. P. D'Evelyn, R. H. Hauge, and J. L. Margrave, in *Diamond, Silicon Carbide and Related Wide Bandgap Semiconductors,* Vol. 162 of *Symposium Proceedings, Series,* edited by J. T. Glass, R. Messier, and N. Fujimori (Materials Research Society, Pittsburgh, PA, 1990), p. 85.
[118]R. E. Shroder, R. J. Nemanich, and J. T. Glass, Phys. Rev. B **41**, 3738 (1990).
[119]B. B. Pate, Surf. Sci. **165**, 83 (1986).
[120]L. H. Robins, L. P. Cook, E. N. Farabaugh, and A. Feldman, Phys. Rev. B **39**, 13 367 (1989).
[121]B. V. Spitsyn, L. L. Bouilov, and B. V. Derjaguin, J. Cryst. Growth **52**, 219 (1981).
[122]T. R. Anthony, Ref. 117, p. 61.
[123]Y. Hirose, S. Amanuma, N. Okaba, and K. Komaki, Ref. 3, p. 80.
[124]Y. Liou, R. Weimer, D. Knight, and R. Messier, Appl. Phys. Lett. **56**, 437 (1990).
[125]W. A. Carrington, L. M. Hanssen, K. A. Snail, D. B. Oakes, and J. E. Butler, Metall. Trans. A **20**, 1282 (1989).
[126]Y. Tzeng, C. Cutshaw, R. Phillips, T. Srivinyunon, A. Ibrahim, and B. H. Loo, Appl. Phys. Lett. **56**, 134 (1990).
[127]M. Frenklach and H. Wang, *Diamond Technology Initiative Symposium* (Strategic Defence Initiative Organization Office of Innovative Science and Technology, Office of Naval Research, Crystal City, VA, 1989), paper T10.
[128]S. J. Harris and A. M. Weiner, Appl. Phys. Lett. **55**, 2179 (1989).
[129]M. Frenklach and E. D. Feigelson, Astrophys. J. **341**, 372 (1989).
[130]M. Frenklach, Ref. 40, p. 1075.